

SPACE SCIENCES LABORATORY

DETAILED FINAL REPORT

Contract NAS 5-24166

EXPERIMENT DEFINITION AND INTEGRATION STUDY
FOR THE ACCOMMODATION OF GIANT,
PASSIVE DETECTOR OF
EXOTIC PARTICLES IN THE COSMIC RAYS (EPIC)
PAYLOAD ON SHUTTLE/SPACELAB MISSIONS

Principal Investigator

Professor P. Buford Price

Period of Performance

June 6, 1977 to February 5, 1978

June 1, 1978

Space Sciences Laboratory Series 19, Issue 37

159895 UNIVERSITY OF CALIFORNIA, BERKELEY

(NASA-CR-~~156842~~) EXPERIMENT DEFINITION AND
INTEGRATION STUDY FOR THE ACCOMMODATION OF
GIANT, PASSIVE DETECTOR OF EXOTIC PARTICLES
IN THE COSMIC RAYS (EPIC) PAYLOAD ON
SHUTTLE/SPACELAB MISSIONS (California

N78-34025

Unclas
33666

G3/93

Space Sciences Laboratory
University of California
Berkeley, California 94720

National Aeronautics and Space Administration

Contract NAS 5-24166

DETAILED FINAL REPORT

EXPERIMENT DEFINITION AND INTEGRATION STUDY FOR THE
ACCOMMODATION OF GIANT, PASSIVE DETECTOR OF
EXOTIC PARTICLES IN THE COSMIC RAYS (EPIC) PAYLOAD
ON SHUTTLE/SPACELAB MISSIONS

Principal Investigator

Professor P. Buford Price

Period of Performance

June 6, 1977 to February 5, 1978

June 1, 1978

Space Sciences Laboratory Series 19, Issue 37

C O N T E N T S

(Contents of Engineering Study follow p. 20)

	<u>Page</u>
I. Conclusions	1
1. Design of EPIC	1
2. Simplicity and low cost	1
3. Feasibility	2
4. Recommendation	2
II. Scientific Study of the EPIC Detector System	2
1. Scientific Goals and Justification of a Huge Detector	2
1.1 Other cosmic ray experiments with large collecting power	2
1.2 Scientific justification for a huge, high-resolution detector	4
2. Study of Detectors	5
2.1 Comparison of various plastic detectors	5
2.2 Sensitivity of CR-39 and Lexan	6
2.3 Resolution of CR-39 and Lexan	7
2.4 Stability of CR-39 and Lexan	8
2.5 Evaluation of CR-39 plastic from various manufacturers	9
3. Design of the Detector Stack	11
4. Automated Track Location and Measurement	12
4.1 Computer-controlled scanning stage	12
4.2 Vidicon-camera for track measurements	13
4.3 Advantages of automation	
5. Recommendations for Further Research and Development	14
References	15
Figures	16

ORIGINAL PAGE IS
OF POOR QUALITY

I. Conclusions

1. Design of EPIC

The EPIC experiment consists of an array of interleaved CR-39 and Lexan track-recording plastic detectors mounted on four rectangular platforms hinged so that the total area in the deployed configuration is 15' x 110'. The volume in detectors is 12' x 96' x 10 g/cm², including trapped radiation shielding and internal, metal absorbing layers. The total weight of the detector assembly plus supporting structure and accessories is 32,000 lb. The modular construction permits as little as one-fourth of the payload to be exposed at a time. The CR-39 is a new type of detector with resolution expected to be comparable to that of the best electronic instruments and with sensitivity adequate to detect and study cosmic rays ranging from minimum-ionizing iron-group nuclei to the heaviest elements. Lexan, with its lower sensitivity but thoroughly proven performance, will be especially useful in studying the rarest, heaviest nuclei.

2. Simplicity and low cost

We have reason to believe that the cost of scientific analysis can be made relatively low by partially automating track location and measurement. Some degree of automation is possible for CR-39 because of the uniquely high clarity, quality, and contrast of etched tracks in this substance. Several engineering design features make the construction of the payload economical. Virtually no attention need be paid to the array during the approximately one year in which it will freely orbit the earth.

ORIGINAL PAGE IS
OF POOR QUALITY

3. Feasibility

Straightforward engineering design permits this detector of unprecedented collecting power -- approximately 150 m^2 -- to be mounted in a retracted configuration within Shuttle, deployed in an extended configuration in space, and recovered for return to earth in retracted configuration.

The detectors will survive a one year exposure to the trapped protons without losing their resolution. The combination of Lexan and the CR-39 detector, with its high resolution and sensitivity, enables us to combine the advantages of passive detectors (low cost, huge collecting power) with the resolution previously attainable only with electronic detectors.

4. Recommendation

Exciting scientific results are sure to be obtained. The huge collecting power may lead to a major discovery. The technology is straightforward. The cost is low. The EPIC experiment should be flown on an early Shuttle mission:

II. Scientific Study of the EPIC Detector System

1. Scientific Goals and Justification of a Huge Detector

1.1 Other cosmic ray experiments with large collecting power

The largest single experiment to date was a stack of Lexan plastic detectors of area 1.2 m^2 exposed inside a 1 g/cm^2 Al wall of Skylab for 253 days at an orbital inclination of $\sim 52^\circ$ and altitude of $\sim 430 \text{ km}$. In that experiment our group (ref. 1*) identified 104 cosmic ray nuclei with $Z \geq 65$, including seven nuclei with $Z \geq 90$, three of which had $Z \geq 94$.

*References for the scientific study begin on page 15.

We found no nuclei with $Z > 96$. The median error in charge was 3.1% or $\Delta Z \approx 2.5$ for the highest charges.

Stacks of Lexan, usually including a few layers of nuclear emulsion, have been exposed on numerous balloon flights at northern U.S. latitudes by groups at Berkeley, Houston, St. Louis, Bristol, and Dublin. The results are summarized in refs. 1 to 3. The charge resolution and total number of nuclei with $Z \geq 65$ were comparable to those for Skylab. About twice as many nuclei with $Z \geq 90$ were reported as were found on Skylab. One unique event that might have been a superheavy nucleus with $Z \approx 114$ or a heavy antinucleus was reported.²

The total area-time-solid angle factor to date for very high rigidity nuclei is $\sim 6 \text{ m}^2 \text{ y ster}$; for particles with rigidity adequate to reach northern U.S. balloon-borne detectors it is $\sim 2.4 \text{ m}^2 \text{ y ster}$.

Fowler's spherical electronic detector, to be flown in the UK-6 satellite in ~ 1980 , will have a collecting power of $\sim 2 \text{ m}^2 \text{ y ster}$ but no better charge resolution than plastic detectors. The HEAO-3 detector of Israel, Waddington, and Stone, to be launched in late 1979, has a $6 \text{ m}^2 \text{ ster}$ collecting power and is believed to have a resolution of ~ 0.4 charge for the heaviest elements. Assuming one year exposures, the UK-6 and HEAO-3 detectors will more than double the present world data on ultra-heavy nuclei and should, with the better resolution of HEAO-3, give us a greatly improved picture of the charge distribution from Fe through Cm ($Z = 26$ to 96). The collecting power will be inadequate to determine the abundance of very rare elements such as the odd- Z nuclei, and the statistics for $Z \geq 90$ will be small.

The Dublin group will expose a 20 m^2 plastic stack on the LDEF satellite in 1980, giving a collecting power of $\sim 40 \text{ m}^2 \text{ y ster}$. Because of the

unfavorable orbit of LDEF, 28.5° , it will detect only highly relativistic nuclei. Its collecting power will be only $\sim 10\%$ that of balloons at northern latitudes and only $\sim 25\%$ that of a satellite at 52° inclination, such as Skylab. We have discussed with the Dublin group the capabilities of our new, high-resolution plastic detector called CR-39, and they will probably use some of it in their experiment.

We conclude that by the end of 1980 one experiment (on HEAO-3), with much higher resolution than Lexan detectors, will have improved the statistics on ultraheavy nuclei by a factor of ~ 2 , and that the LDEF experiment can improve the statistics by another factor of about five, when its unfavorable orbit and proximity to solar maximum are taken into account. These data may be of high quality if the new CR-39 plastic is utilized.

1.2 Scientific justification for a huge, high-resolution detector

The determination of the charge distribution of the ultra-heavy cosmic rays with high resolution and good statistics has been repeatedly cited by high-energy astronomy and Shuttle study groups as a high-priority goal for the Shuttle era. Only part of the problem will be solved by presently planned experiments: HEAO-3 will have the resolution but will not obtain enough events to determine the abundances of ultraheavy odd-Z nuclei nor the relative abundances of the transuranic nuclides.

What is needed is an experiment with a factor $\sim 10^2$ improvement in collecting power over Skylab and HEAO-3 and charge resolution at least as good as that of HEAO-3. We show in this report that such an experiment is feasible and surprisingly inexpensive.

In addition to the definite payoff in improved understanding of nucleosynthesis and cosmic ray astrophysics that will come from such an

experiment, a strong motivating factor is the possibility of discovering entirely new classes of particles whose existence would greatly influence physics, astrophysics, and possibly cosmology. Such particles include:

- a. Superheavy elements, with $Z \gtrsim 110$
- b. Magnetic monopoles
- c. Heavy anti-nuclei
- d. Abnormally dense, highly charged, massive particles such as discussed by Lee and Wick, by Bodmer, and by Migdal
- e. Highly charged subnucleons, proposed by Yock

Our group, with our Houston collaborators, has completed our study of the particle we first attributed to a magnetic monopole. A detailed paper has appeared as an LBL report and will soon be published in the Physical Review. New evidence, from two emulsion layers not studied at the time of the first paper, confirms the observation that the particle produced far fewer high-energy delta rays than expected if it were an ordinary nucleus with $Z \lesssim 96$. Detailed calibrations of the Lexan stack and of the emulsion layers were presented. We retracted the claim that the particle was a monopole, showed that it was compatible with a highly relativistic nucleus with $Z \approx 110$ to 114 or with an ultraheavy antinucleus, and showed that it appears not to have been a normal nucleus with $Z \lesssim 96$. An experiment with greatly increased collecting power might detect many more of such peculiar particles and establish their identity.

2. Study of Detectors

2.1 Comparison of various plastic detectors

In the table below we compare the characteristics of Lexan polycarbonate, cellulose nitrate and acetate, and CR-39 ally diglycol

carbonate. The cellulosic polymers are unsuitable for many reasons and will not be considered further. The properties of Lexan as a particle detector have been known for some years.⁴ Our group recently discovered the extraordinary properties of CR-39 as a particle detector.⁵

Characteristic	Lexan	Cellulosic plastic	CR-39
Optical quality of etched track	good	poor	excellent
Minimum detectable value of Z/β	~ 65	~ 32	~ 10
Fractional standard deviation in response	$\sim 4\%$	poor	$\sim 1\%$
Stability	requires a few mbars O_2 and $T < 40^\circ C$	unstable	keep trapped particle dose $\leq 5 \times 10^8 / cm^2$ and $T < 40^\circ C$

Figures 1, 2, and 3 show that etched tracks in CR-39 have extraordinary contrast and optical quality. We later discuss a method for automatically measuring these tracks. In the next subsections we discuss sensitivity, resolution, and stability of Lexan and CR-39, the two plastics we propose for the EPIC experiment.

2.2 Sensitivity of CR-39 and Lexan

Figure 2 shows etched tracks of $14 \text{ MeV/nucleon } ^3\text{He}$ ions in CR-39. We irradiated the sample at normal incidence, so the etch pits have a circular shape. The value of Z/β for these ions is 11.8. Lexan records ions with Z/β only above ~ 65 . Figure 4 shows quantitative curves of response, defined as the ratio of track etch rate to bulk etch rate, for CR-39 and Lexan. The much higher sensitivity of CR-39 makes possible the study of minimum-ionizing nuclei in the region between $Z = 26$ and 65, which

is inaccessible to Lexan.

Relativistic ($\beta \approx 1$) nuclei with $Z \gtrsim 90$ will produce extremely long tracks in CR-39. It will be very useful to interleave occasional Lexan sheets so that these events can be quickly located and the regions of CR-39 through which they passed can be etched for a shorter time than normal.

2.3 Resolution of CR-39 and Lexan

Our studies of the resolution of Lexan, reported in refs. 1 and 2, have shown that the fractional standard deviation in etch rate is from ~ 3 to $\sim 8\%$ and is typically $\sim 4\%$ for relativistic ultraheavy nuclei. Experiments in progress suggest that there may be ways to reduce this figure to ~ 2 to 3% . This is adequate to determine whether we have detected a superheavy nucleus ($Z \approx 110$ to 114) but is inadequate to allow us to improve on the expected results of the HEAO-3 experiment using Lexan alone.

In ref. 5 we reported that the resolution of CR-39 from one manufacturer (Polytech, Inc.) was $\sim 1.3\%$ for 600 MeV/nucleon Fe nuclei at normal incidence, but that a decrease of sensitivity in the interior of each sheet resulted in a variation of response with angle of entry. In Figures 3 and 5 of this report we show the results of a study of resolution of carbon and nitrogen ions in a batch of CR-39 made in a slightly different way by the same firm. The depth dependence has been eliminated, but there is a variability of about 4% from sheet to sheet that can be corrected for by accelerator calibrations. The resolution of a given sheet is spectacular. We used a Vidicon camera to measure the area of the circular etch pit at each event. If the bulk etch rate is known, the diameter or area of the etched track is a measure of the track etch rate. The histograms in Figure 5 show that 32 MeV/nucleon ^{12}C and ^{14}N are separated by $\sim 14\sigma$. At the bottom

of the 1.5 mm CR-39 sheet, histograms of etch pit areas, shown at the bottom of Figure 5, are separated by $\sim 20\sigma$. For particles of unknown energy and arbitrary angle of entry the separation would not be as good, but these tests indicate that CR-39 probably has resolution competitive with the best electronic detectors and far exceeding that of Lexan.

2.4 Stability of CR-39 and Lexan

Our group found⁶ that Lexan exposed in the high vacuum of space has a much lower sensitivity than that exposed in a partial pressure of oxygen. Lexan exposed in the moderate vacuum typical of accelerators ($\sim 10^{-5}$ torr) shows no loss of sensitivity. Sealing a stack containing Lexan in a bag containing air at a pressure exceeding 10^{-3} torr should insure a normal response. CR-39 also seems to record tracks normally at pressures as low as $\sim 10^{-5}$ torr.

Latent images of tracks fade in both Lexan and CR-39 at rates that increase exponentially as $\exp(-U/kT)$, where $U \approx 1$ eV. During a one-year space exposure a passive thermal control paint would keep the temperature between 23°F and 35°F (or -5°C to 2°C).

Lexan exposed outside the Skylab⁶ showed no degradation due to accumulated exposure to trapped protons. Using 25 MeV protons we have simulated exposures of CR-39 to the trapped radiation. After first bombarding four sheets of CR-39 with 32 MeV/nucleon ^{12}C and ^{14}N , we next bombarded these sheets with 3×10^8 , 10^9 , 10^{10} , and 10^{11} protons/cm² respectively. These protons did not directly record tracks but produced a background of short, recoil proton tracks due to collisions with hydrogen in the CR-39. The effect of ionization by the incident protons was undetectable. The carbon and nitrogen tracks could easily be seen and measured in the

sheet exposed to 3×10^8 protons of 25 MeV but not in the most heavily irradiated sheets. We recommend that CR-39 not be exposed to more than $\sim 5 \times 10^8/\text{cm}^2$ trapped protons.

At solar maximum, the nominal average flux of trapped protons integrated along various orbits for one year is summarized below:⁷

Altitude	30° Orbit		60° Orbit	
	Flux($\text{cm}^{-2}\text{y}^{-1}$) ($E \geq 10$ MeV)	Flux ($E \geq 50$ MeV)	Flux ($E \geq 10$ MeV)	Flux ($E \geq 50$ MeV)
150 n.m.	5×10^6	4×10^6	1.7×10^7	1.3×10^7
225 n.m.	8×10^7	7×10^7	1.5×10^8	1×10^8
300 n.m.	1.5×10^9	1×10^9	1×10^9	7×10^8

The trapped flux falls off very steeply with altitude. At altitudes up to about 250 nautical miles the flux integrated over one year is low enough not to provide a serious background problem for CR-39. In the engineering section of this report we assumed a final altitude of 160 n.m. and calculated that the initial altitude for a one year exposure would have to be 238 n.m. We thus conclude that trapped protons with energies above 10 MeV will not affect the EPIC experiment. To exclude low energy protons we propose to employ copper shielding ~ 1 mm thick above and below the plastic detector stacks. This will stop protons up to ~ 25 MeV.

2.5 Evaluation of CR-39 plastic from various manufacturers

We have encountered the usual barriers of proprietary secrecy in dealing with representatives of the various companies that make sheets of CR-39. Three firms have cooperated with us in our efforts to optimize the performance of commercially available sheets. These are SGL Homalite Corp., Wilmington, Del.; Polytech, Inc., Owensville, Mo.; and Pershore Mouldings, Ltd., Pershore, Worcestershire, U.K.

Samples of CR-39 from different sources differ significantly in quality as a particle identifier. The major variables are quality of the liquid monomer; percentage and type of initiator; type of mold release agent and UV stabilizer; percentage of copolymer; cure temperature cycle; and method of curing.

American firms use the monomer supplied by Pittsburgh Plate Glass. It contains varying amounts of volatiles and is nominally of $\geq 95\%$ purity. To improve quality control, it might be useful to employ several stages of both distillation and filtration. All firms use ~ 2 to 3% of diisopropyl peroxydicarbonate initiator. Cure times range from 12 to about 36 hours. The cycle of temperatures and times is proprietary.

Commonly used copolymer additives are vinyl acetate and methyl methacrylate. Vinyl acetate additive gives no difficulties, but as little as 2% of methyl methacrylate leads to etched tracks that are filled with an insoluble, gummy residue, with disastrous results. Some batches of CR-39 made without any deliberate copolymer lead to tracks filled with a similar gummy residue. The gummy layer acts as a barrier to diffusion of reactants away from the etched track and of solvent into the track. All three firms are willing to supply CR-39 without copolymer upon request.

The British firm cures its CR-39 sheets in a vertical mold in a hot water bath. The American firms use horizontal molds in air ovens. We have found gradients of $\sim 3\%$ per inch in track etch rate along sheets made by the British firm, probably because of gradients built in during curing in the vertical mold. They are now planning to make us samples cured in a horizontal mold.

Several samples we tested showed extremely high uniformity in the plane of the sheet but a large, depth-dependent decrease in chemical reactivity from a maximum at each surface to a minimum in the center. Some samples showed asymmetric gradients across the thickness. Only a few samples showed no detectable gradients. Etch rate gradients can be studied either by bombarding with high-energy heavy ions that penetrate the sheet or by preparing a "taper section" (imbedding the sheet in epoxy, grinding at an angle and polishing it), irradiating with monoenergetic charged particles, etching, scanning along the taper section with a microscope, and looking for gradients in the size of the etch pits. No large order should be placed without first establishing by direct measurement of tracks that a sample supplied by the firm is free of gradients in chemical reactivity.

The one factor that presently limits our ability to specify a standard production method is the variability of the liquid monomer supplied to the casting firms by Pittsburgh Plate Glass. We are continuing to work with the three casting firms to achieve a standardized procedure for mass production of high-resolution CR-39 detectors.

3. Design of the Detector Stack

The stack will consist of identical individual modules of area 16" x 16" arrayed side by side over a total active area 12' x 96' and with thickness $\sim 10 \text{ g/cm}^2$. Each module contains the following components:

- a. Copper sheet 1 mm thick (0.9 g/cm^2) above and below the active detector sheets. The copper prevents trapped protons below $\sim 25 \text{ MeV}$ from reaching the detectors. The outside surfaces will be painted with thermal control paint as discussed in the engineering section.

b. CR-39 sheets, each 1.5 mm thick (0.2 g/cm^2), interleaved with Lexan sheets, each 0.25 mm thick (0.03 g/cm^2). The Lexan will be used mainly to single out the most highly ionizing particles and to measure events near and well beyond uranium, where it would be less convenient to use CR-39. The total thickness in active detectors will be 3 g/cm^2 of CR-39 and 0.9 g/cm^2 of Lexan.

c. Copper absorber sheets, each 0.9 g/cm^2 . Five of these will be interleaved at uniform intervals between sub-stacks of CR-39 and Lexan. The function of the copper is to slow the heavy nuclei without breaking them up. High-Z material is far more effective than plastic in its ability to slow nuclei nondestructively.

d. A plastic envelope sealed around each module. The bag maintains a pressure of ≥ 1 mbar of air at each detector. Lexan loses its sensitivity at the low ambient air pressure of space. Any concentration of air above $\sim 10^{-4}$ torr is probably adequate to ensure a sufficient level of O_2 dissolved in the Lexan to give good track registration.

4. Automated Track Location and Measurement

4.1 Computer-controlled scanning stage

The clarity and high contrast of etch tracks in CR-39 (Figs. 1-3) make possible automated methods of track location and measurement. To locate a track that penetrates one of the $16'' \times 16'' \times 1.5 \text{ mm}$ CR-39 sheets we propose to detect light scattered from the etch pits on the top and bottom surfaces, with a laser beam as the light source. The stack will be accurately machined. Successive sheets will be inspected in a standard

position on the scanning stage, and the shift in location and intensity of the signal from the etch pits from sheet to sheet will provide the zenith angle of the particle and rough measures of its dE/dx and rate of change of dE/dx with depth. Events that satisfy specified criteria will have their positions stored in our PDP 11/40 computer for later measurement.

We are building a small-scale prototype consisting of a 13" stage positionable to 10^{-3} cm.

4.2 Vidicon-camera for track measurements

Simple tests with an inexpensive, commercially available Vidicon show that we can measure the areas of vertical etch pits very reproducibly. Figures 3 and 5 show some of the results. A knowledge of etch pit area at the plastic surface, together with zenith angle and stopping depth, suffice in principle to identify a particle not too heavily ionizing. In practice we would measure several etch pit areas at different points along the particle's range so as to improve our resolution.

Very heavily ionizing particles lead to very long etch pits for which the area at the surface is not a sensitive measure of dE/dx . We are working on a method of using the Vidicon to measure etch pit depth for an arbitrary zenith angle. By using a Nomarski interference contrast attachment on a Zeiss microscope we believe it may be possible, with a Vidicon, to focus on a "slice" through the etch pit that can be measured and its centroid determined. We would then take several slices at different, equally spaced depths and determine the shift of centroid with depth, thus converging on the location of the tip of the etch pit and giving the length and zenith angle of the etch pit.

4.3 Advantages of automation

The main cost of our Skylab experiment was labor. Automation would enable us to handle the much greater volume of information in the present experiment at a cost comparable to that of Skylab.

5. Recommendations for Further Research and Development

It is not yet possible to buy CR-39 sheets that are guaranteed to give 1% resolution over their entire area. Additional funds are needed to continue a program of cooperative development with the several manufacturers.

It would be highly desirable to have a Vidicon system, with appropriate microscope optics, capable of automated measurements of track dimensions. Additional funds are needed to complete the development of such a system.

Because of the limited funds, we have been unable to make a detailed cost estimate in the present study.

References

1. E.K. Shirk and P.B. Price, *Astrophys. J.*, 220, 719 (1978).
2. P.B. Price, E.K. Shirk, W.Z. Osborne and L.S. Pinsky, LBL Report No. 7198 and *Phys. Rev. D*, to be published.
3. P.H. Fowler, C. Alexandre, V.M. Clapham, D.L. Henshaw, C. O'Ceallaigh, D. O'Sullivan, and A. Thompson, *Nucl. Instr. and Meth.*, 147, 195 (1977).
4. R.L. Fleischer, P.B. Price, and R.M. Walker, Nuclear Tracks in Solids, Univ. of Calif. Press, Berkeley (1975).
5. B.G. Cartwright, E.K. Shirk, and P.B. Price, *Nucl. Instr. and Meth.*, in press (1978).
6. J.H. Chan and P.B. Price, *Phys. Rev. Lett.*, 35, 539 (1975).
7. D.M. Sawyer and J.I. Vette, "AP-8 Trapped Proton Environment for Solar Maximum and Solar Minimum," NSSDC Publication WDC-A-R&S 76-06.

ORIGINAL PAGE IS
OF POOR QUALITY

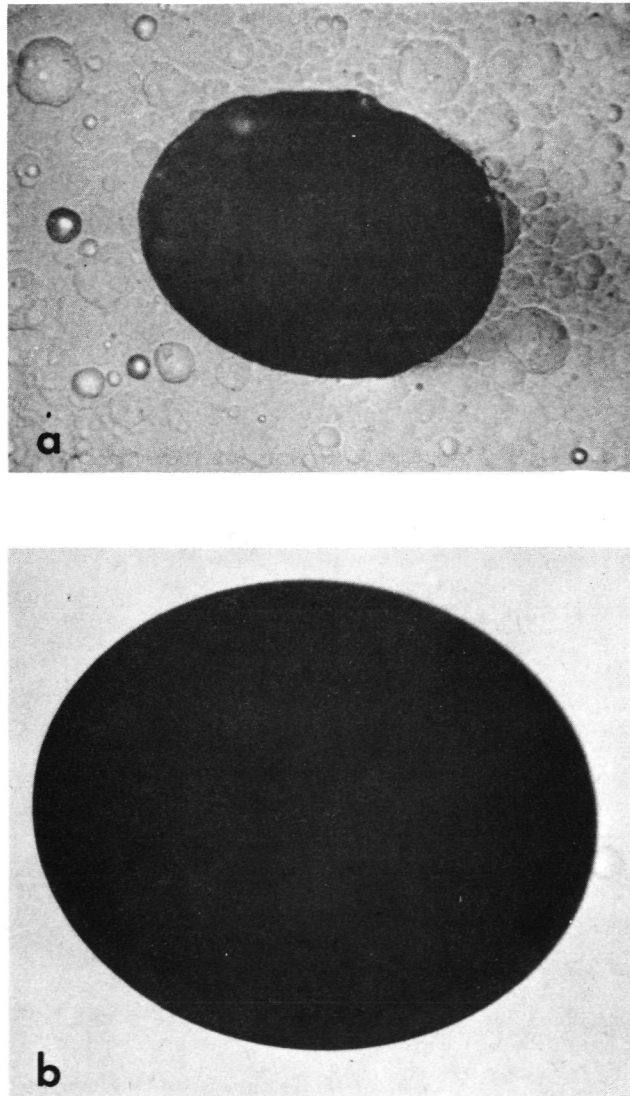


Figure 1. Comparison of surfaces of (a) Lexan and (b) CR-39, etched in NaOH solution. The elliptical holes are the mouths of track etch pits that intersected the surface at an angle. The high quality of the image of the etch pit in CR-39 is obvious.

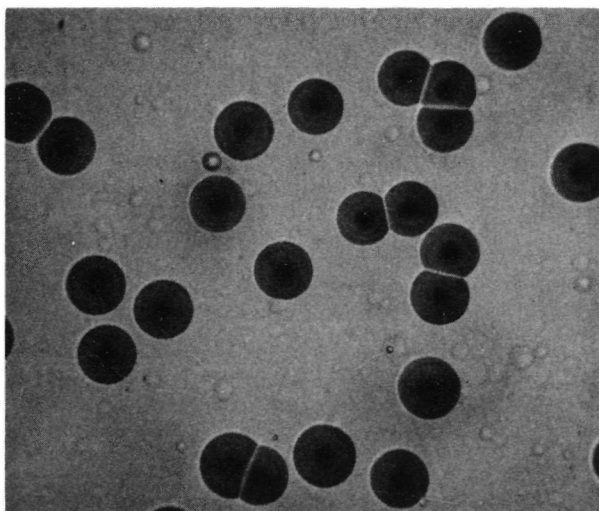


Figure 2. Etch pits of ~ 60 MeV alpha particles ($Z/\beta \approx 10$) illustrating the high sensitivity of CR-39.

ORIGINAL PAGE IS
OF POOR QUALITY

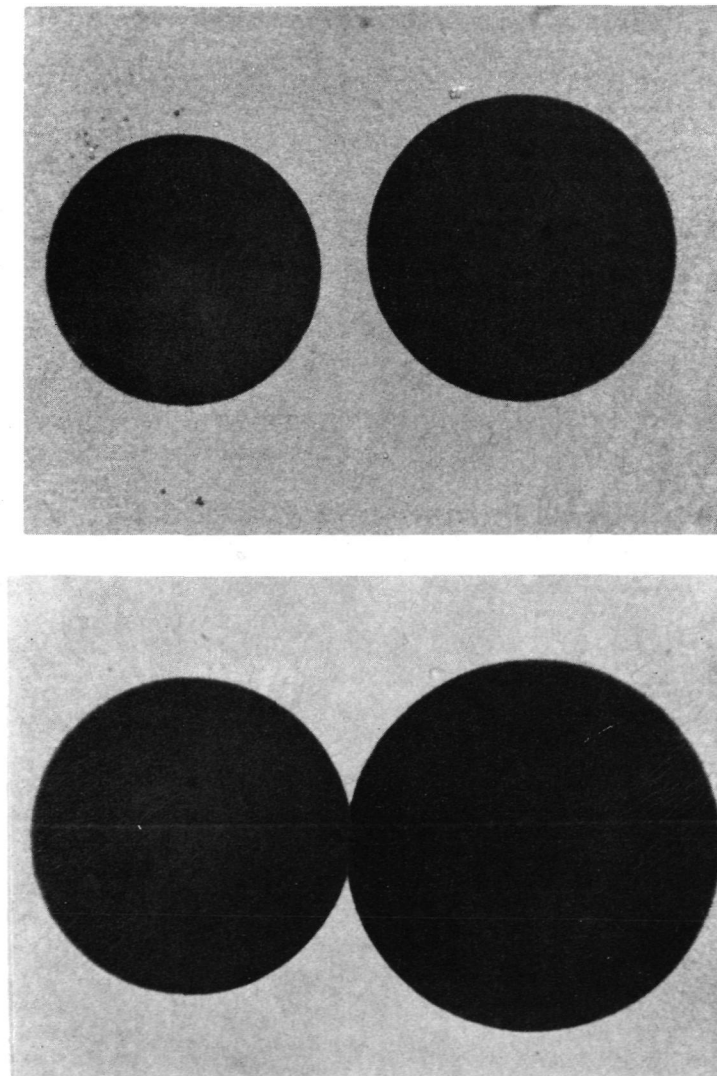


Figure 3. Comparison of the etch pits of ^{12}C ions (left) and ^{14}N ions (right) in CR-39. At top they both have energies of 32 MeV/amu. At bottom they have passed through a 1.5 mm sheet of CR-39. Their clarity and contrast make automated measurements with a Vidicon camera possible (see Figure 5).

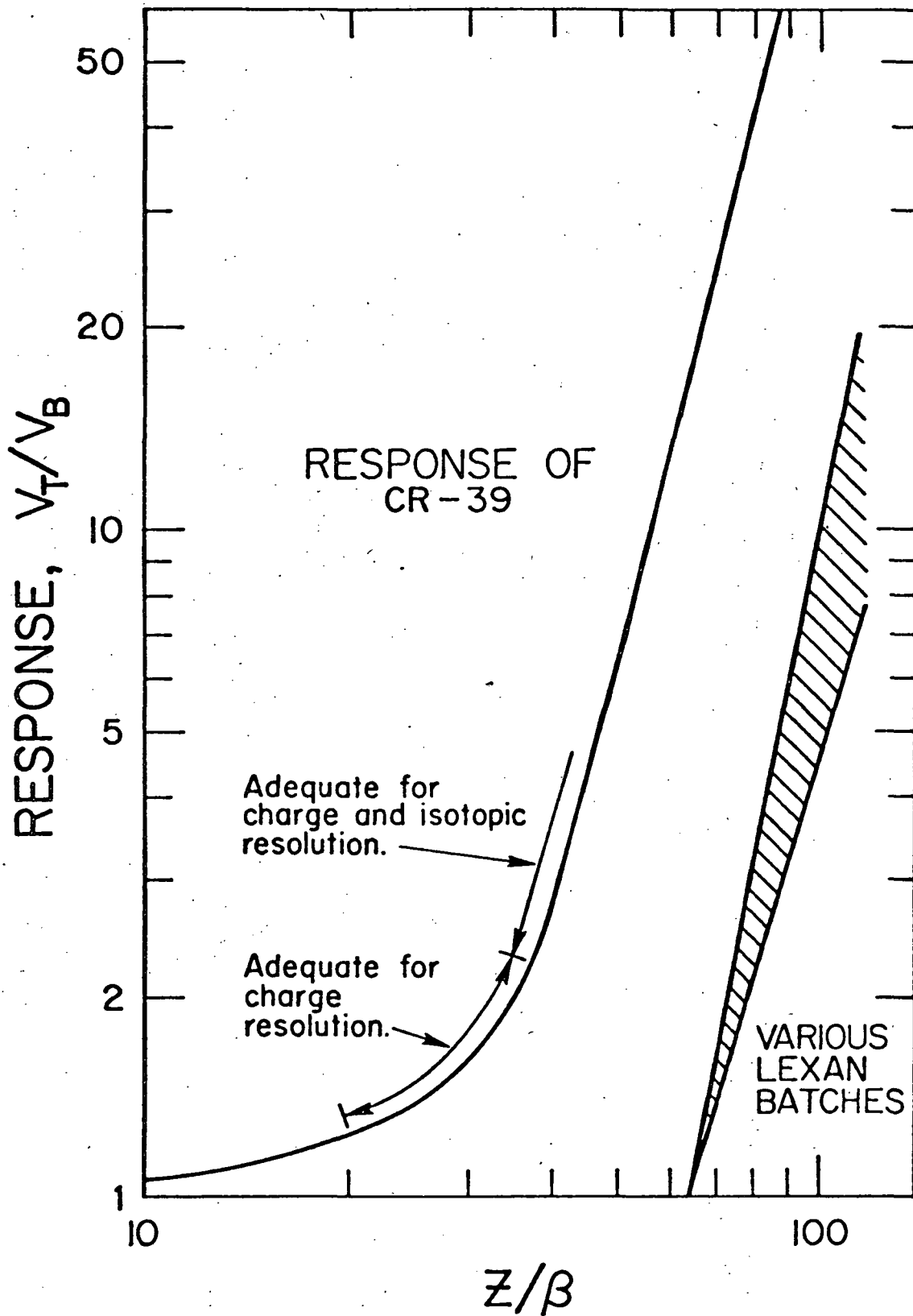


Figure 4. Response of CR-39 and of Lexan as a function of the ratio of charge to velocity, Z/β . The response is defined as ratio of track etch rate to bulk etch rate. The higher sensitivity of CR-39 is obvious.

ORIGINAL PAGE IS
OF POOR QUALITY

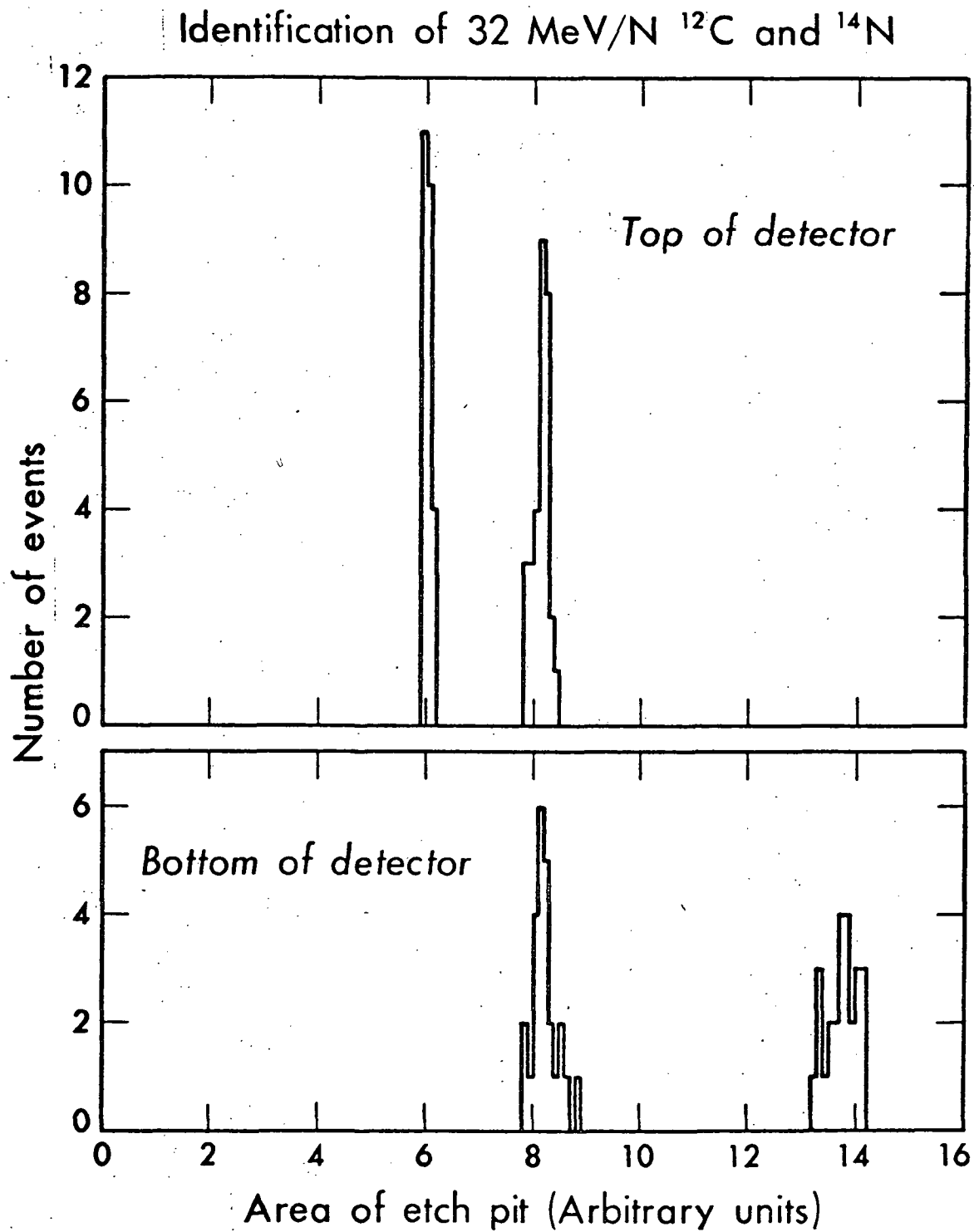


Figure 5. Measurements of etch pit areas for events such as shown in Figure 3, illustrating the high resolution of CR-39.

Space Sciences Laboratory
University of California
Berkeley, California 94720

~~PRECEDING PAGE BLANK NOT FILLED~~

NASA Contract NAS 5-24166

ENGINEERING ASPECTS OF THE
FEASIBILITY OF A GIANT, PASSIVE DETECTOR OF
EXOTIC PARTICLES IN THE COSMIC RAYS (EPIC) PAYLOAD
ON SHUTTLE/SPACELAB MISSIONS

Principal Investigator

Professor P. Buford Price

Prepared by: R.H. Weitzmann

April 21, 1978

C O N T E N T S

Section	Page
1 Introduction	1
2 Description of Payload	2
2.1 Design Approach	2
2.2 Concept and Configuration	2
2.3 Subsystem Descriptions	4
2.3.1 Structure Subsystem	4
2.3.2 Retention Subsystem	8
2.3.3 Panel Deployment/Retraction Subsystem	8
2.3.4 Detector Subsystem	16
2.3.5 Despin Subsystem	16
2.3.6 Telemetry/Command Subsystem	19
2.3.7 Power Subsystem	19
3 Mass Properties	22
3.1 Weight Summary	22
3.2 Center of Gravity Location	24
3.3 Moments of Inertia	24
4 Assembly and Ground Handling	24
5 Testing and Quality Assurance	25
5.1 Structural and Mechanical Testing	25
5.2 Thermal Vacuum Testing	26
5.3 Quality Assurance	26
6 Mission Profile and Flight Sequence Summary	26

<u>Appendices</u>	<u>Page</u>
A-1 Attitude and Orbit Decay	30
A-2 Deployment/Retraction Design Analysis	34
A-2.1 Panel Locking Mechanism Design	34
A-2.2 Panel Deploy/Retract Drive Design	35
A-2.3 Deployment Initiator Mechanism Design	38
A-3 Thermal Design Analysis	39
A-4 Schedule	43
A-5 LDEF Option	44

Illustrations

Figure

2.2-1	"EPIC" Detached Payload, Fully Deployed Configuration	2
2.2-2	"EPIC" Detached Payload, Stowed Configuration	3
2.3.1-1	Basic Panel Structure Details	5
2.3.1-2	Basic Panel Dimensions and Detector Subassembly Arrangement	6
2.3.1-3	Detector Subassembly Frame (Welded Construction)	7
2.3.2-1	5-Point Payload Retention System (Indeterminate)	9
2.3.2-2	Panel Locking Concept in Stowed Configuration	10
2.3.3-1	Redundant Drive Unit Concept	12
2.3.3-2	Deployment/Retraction Mechanism Arrangement	13

2.3.3-3	Deployment Initiator/Retract Clamping Mechanism	15
2.3.4	Detector Detail	17
2.3.6-1	Electrical System Block Diagram	20
2.2.6-2	Deploy/Retract Logic Diagram	21
2.3.7-1	Power Profile	23
A-1	Orbit Decay	32
A-2.2	Torque Requirement of Center Hinge (Retraction)	37
A-6	"EPIC" Passive Detector Mounted in Standard 3-inch LDEF Peripheral Tray Assembly	45

ORIGINAL PAGE IS
OF POOR QUALITY

1 Introduction

This report describes the result of an engineering investigation into the feasibility of design, construction, launch and retrieval, of a giant, passive detector to be placed into circular orbit using the NASA Space Shuttle.

2 Description of Payload

2.1 Design Approach

The design approach was based on the following guidelines:

- Design a structure which can accommodate a maximum number of detector panels compatible with the shuttle return load capacity of 32,000 lb.
- Make the structure compatible with standard shuttle payload accommodation methods and mechanical interfaces.
- Use design concepts, materials, devices, and other technology proven acceptable through in-flight use.
- Minimize complexity of integration and ground handling
- Utilize commercially available standard materials and components to minimize cost.
- Provide passive gravity gradient stability through appropriate, deployed geometry.

2.2 Concept and Configuration

The basic structure will consist of four large, rectangular panels hinged together to form a rectangular array of approximately 15 x 110 feet when fully deployed (Figure 2.2-1). During launch and retrieval, the frames are locked together in the configuration shown in Figure 2.2-2 and secured in the shuttle bay with standard retention and auxiliary fittings. Deployment

ORIGINAL PAGE 1.
OF POOR QUALITY

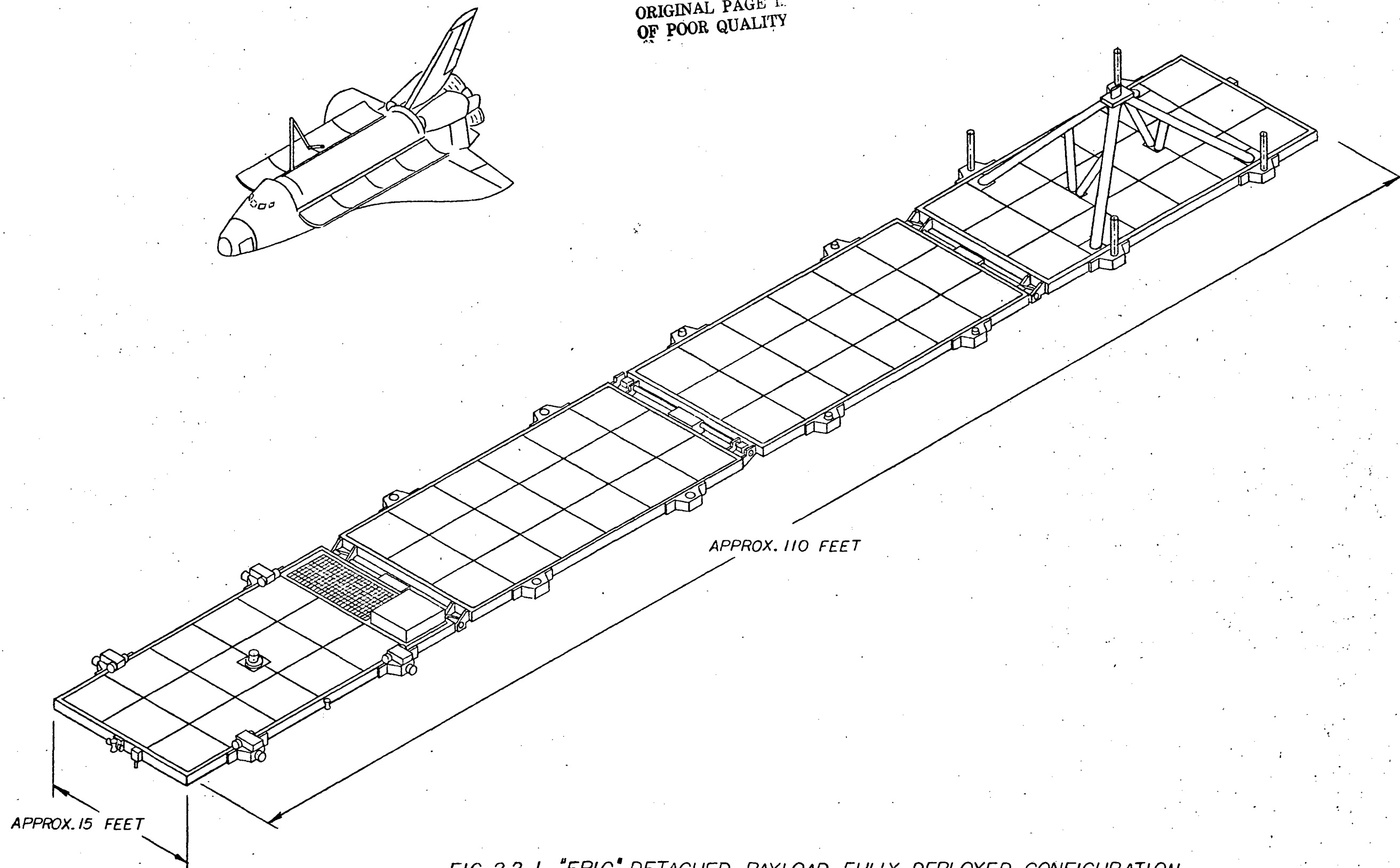
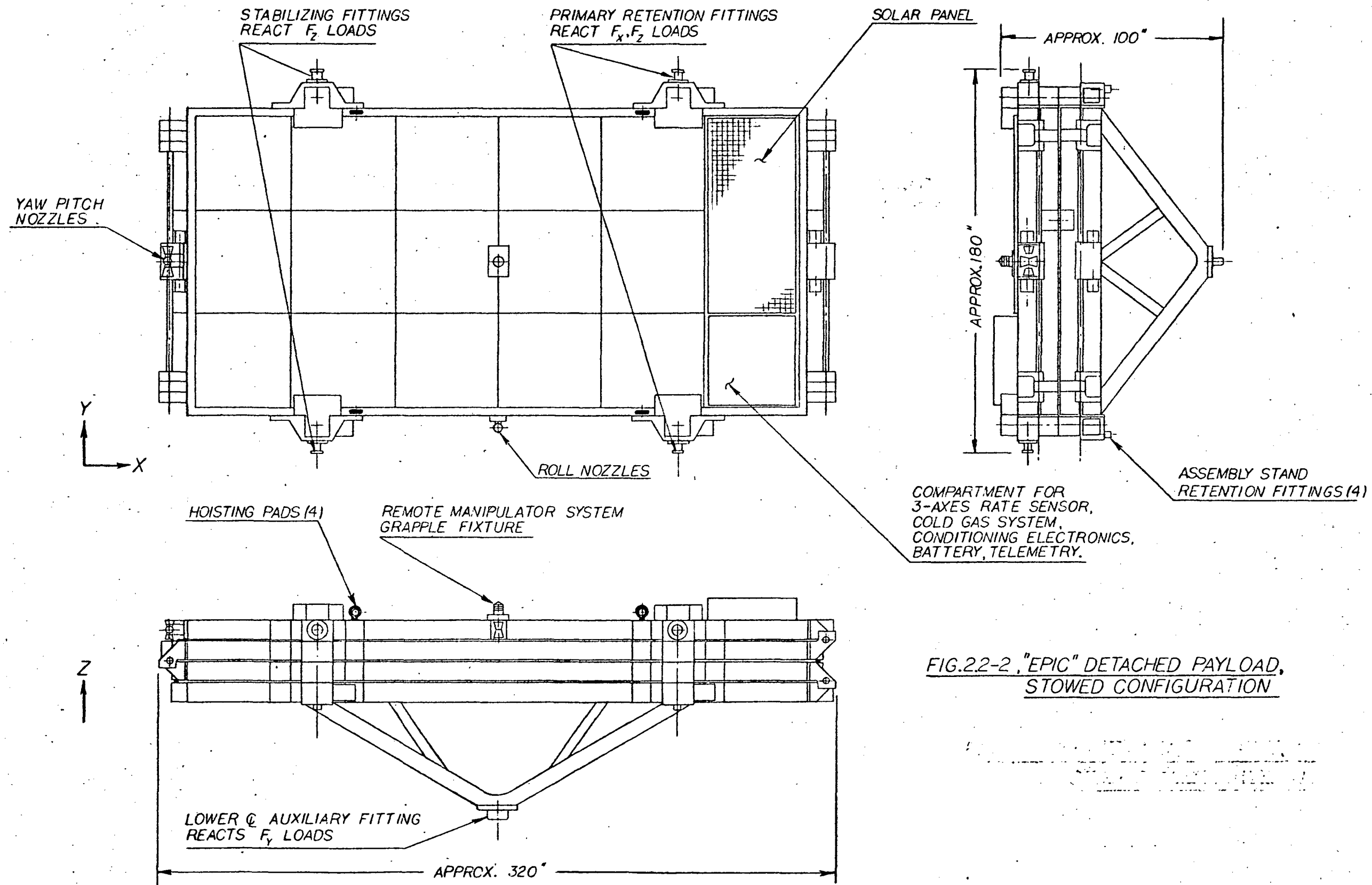


FIG. 2.2-1, "EPIC" DETACHED PAYLOAD, FULLY DEPLOYED CONFIGURATION



and retraction of the panels is accomplished by means of redundant motors at the hinge joints.

In order to reduce motion about the center of mass in the stowed configuration to levels dictated by Shuttle retrieval constraints, a 3-axes rate sensor and cold gas system are used.

Deployment and retrieval of the payload in orbit will utilize the shuttle remote manipulator system attaching to the grapple fixture of the payload identified in Figure 2.2-2.

Required power for panel deployment and retraction functions, attitude control, and receive/transmit telemetry will be provided by batteries, and a small solar cell array providing a trickle charge to the batteries. Major power demands are placed on the batteries at the beginning (panel deployment) and end (panel retraction) of the mission; during the passive period between these functions, only receiver power and occasional transmitting power is required.

2.3 Subsystem Descriptions

2.3.1 Structure Subsystem

Structural details of the four basic panels are shown in Figure 2.3.1-1. The panels will be fabricated from commercially available standard aluminum structural shapes, using 8 x 3.75 x $\frac{1}{4}$ inch channels for the main frame and 6 x 4 x $\frac{3}{16}$ inch I-beams for the interior support structure. For ease of handling, assembly, and to minimize distortion, the individual structural members will be joined through bolted interfaces at all intersections.

Each basic panel will support a total of 18 detector subassemblies in the arrangement shown in Figure 2.3.1-2. The individual detector subassembly, whose welded frame is shown in Figure 2.3.1-3, will be secured with 16 bolts each to the panels. In this way the fully assembled panel configuration

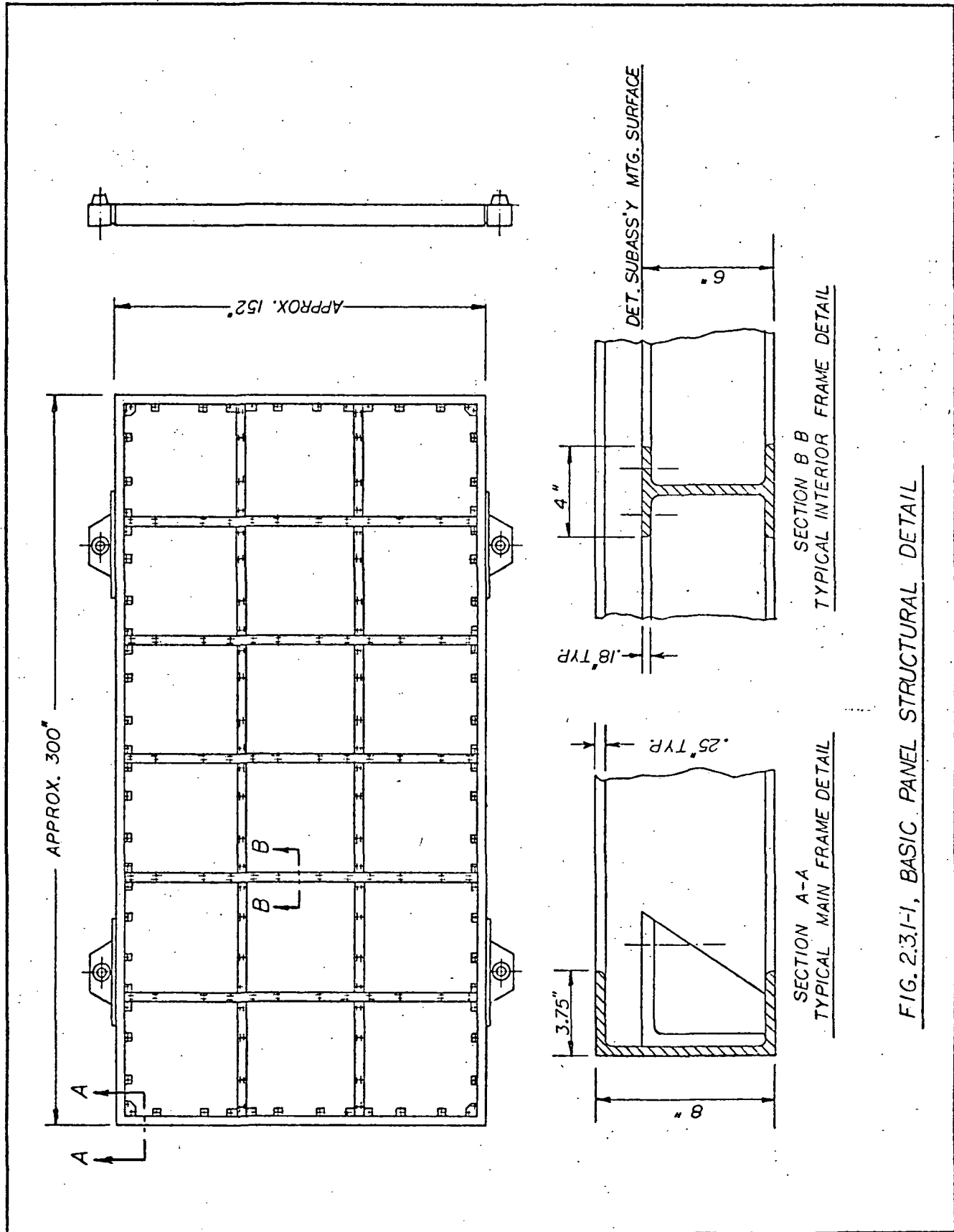


FIG. 2.3.1-I, BASIC PANEL STRUCTURAL DETAIL

ORIGINAL PAGE IS
OF POOR QUALITY

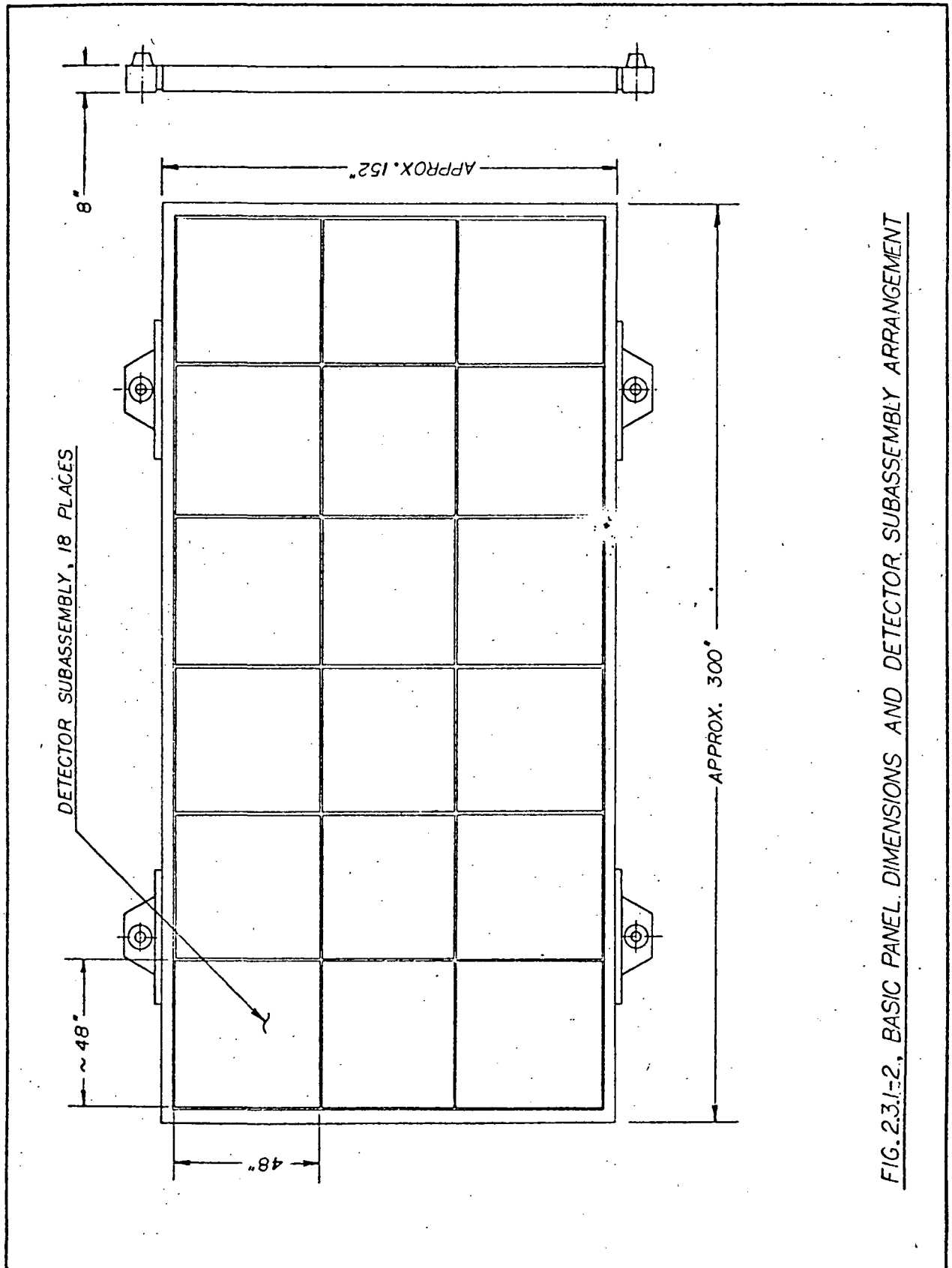


FIG. 2.3.1-2. BASIC PANEL DIMENSIONS AND DETECTOR SUBASSEMBLY ARRANGEMENT

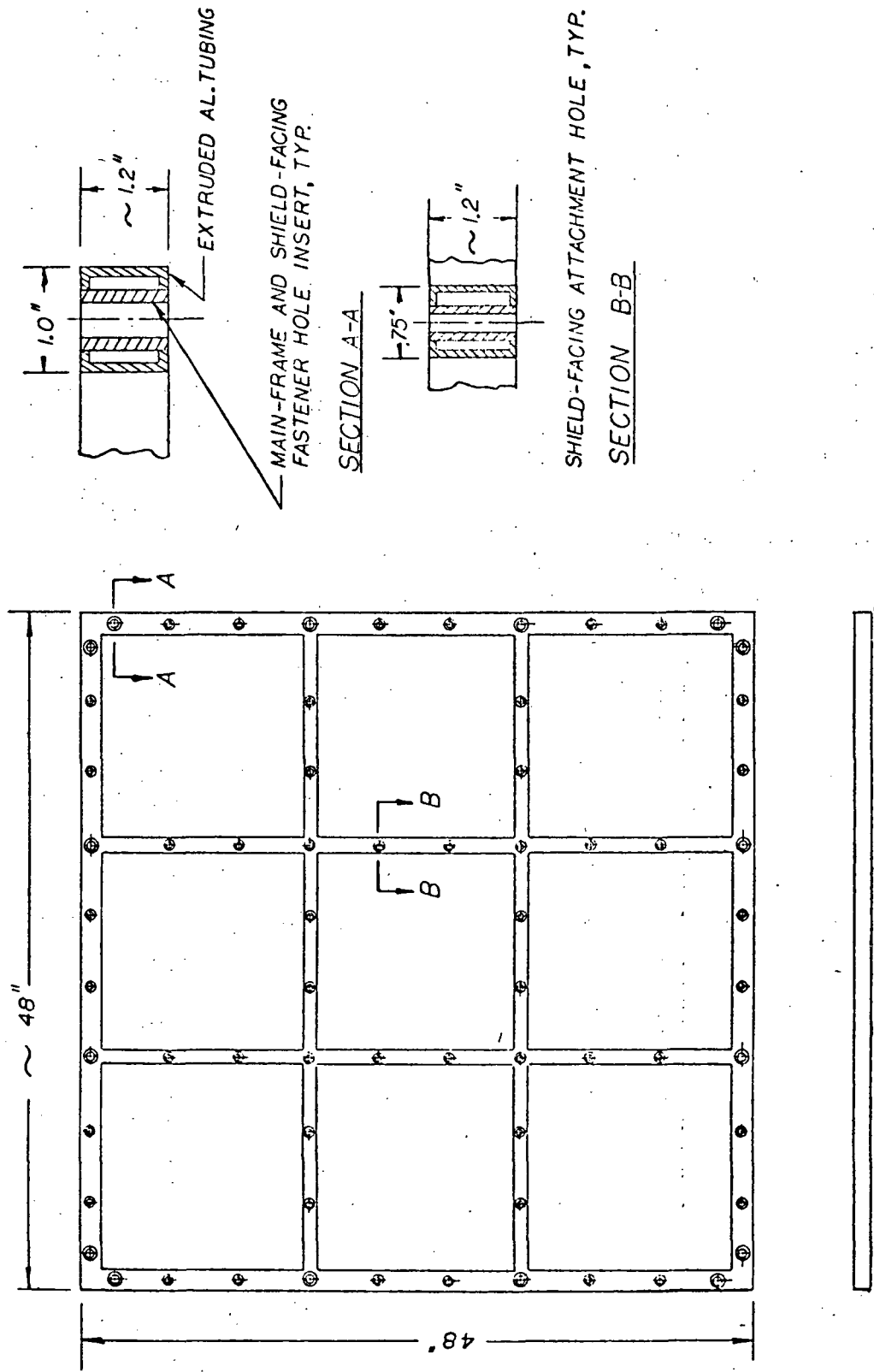


FIG.2.3.1-3, DETECTOR SUBASSEMBLY FRAME (WELDED CONSTRUCTION)

will have very high in-plane structural stiffness. The individual panel weight without detectors will be approximately 750 lbs.

2.3.2 Retention Subsystem

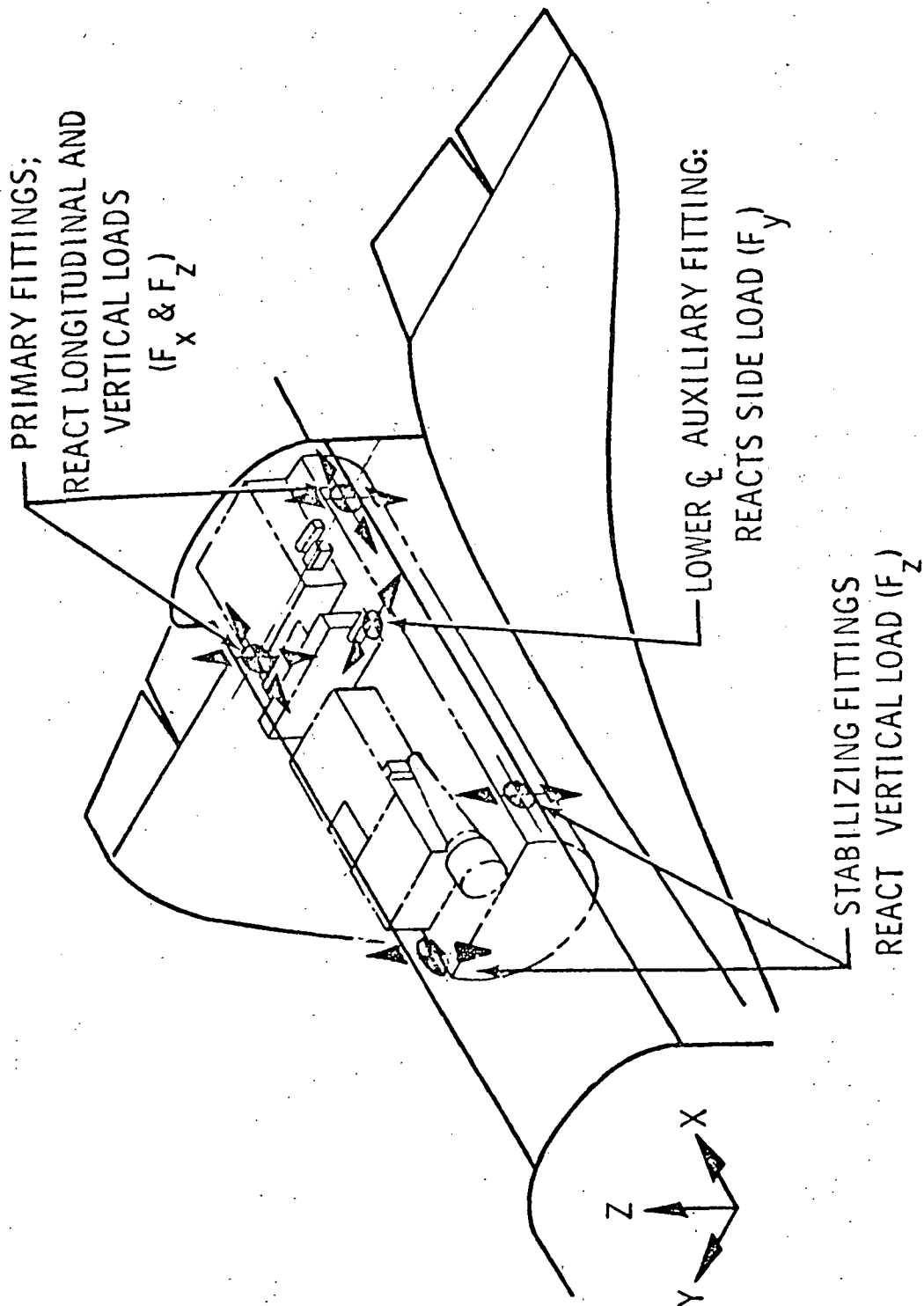
In the stowed configuration the experiment will be mounted in the Shuttle bay utilizing the 5-point payload retention system of volume XIV of the Space Shuttle System Payload Accommodations handbook and repeated here for convenience in Figure 2.3.2-1. The corresponding primary fittings, stabilizing fittings, and auxiliary fittings are identified in Figure 2.2-2.

Static and dynamic payload loads in the X and Z directions are transferred to load adapters bolted to the long sides of each panel. In the stowed configuration these load adapters lock the individual panels together in the manner shown in Figure 2.3.2-2. The conical engagement sections will facilitate alignment during the final motion of the retraction maneuver and assure lateral load capability when locked. A rack-and-pinion driven tie-down bolt, rotationally keyed, serves as the common tension member. The required tension in the tie-down bolt is provided by the motor-driven nut shown. The uppermost load adapters also serve as the mounting surfaces for the longeron trunnions which are the attachment interfaces to the Shuttle retention system.

Experiment Y-loads are transferred through a welded, tubular structure on the underside of the lower-most panel to the lower centerline auxiliary fitting where they are taken up by the Shuttle keel bridge attachment interface.

2.3.3 Panel Deployment/Retraction Subsystem

In orbit, the payload will be released from the Shuttle mounting interface by unlatching the retention system, and separated from the Shuttle with



ORIGINAL PAGE IS
OF POOR QUALITY

FIG. 2.3.2-1 5-POINT PAYLOAD RETENTION SYSTEM (INDETERMINATE)

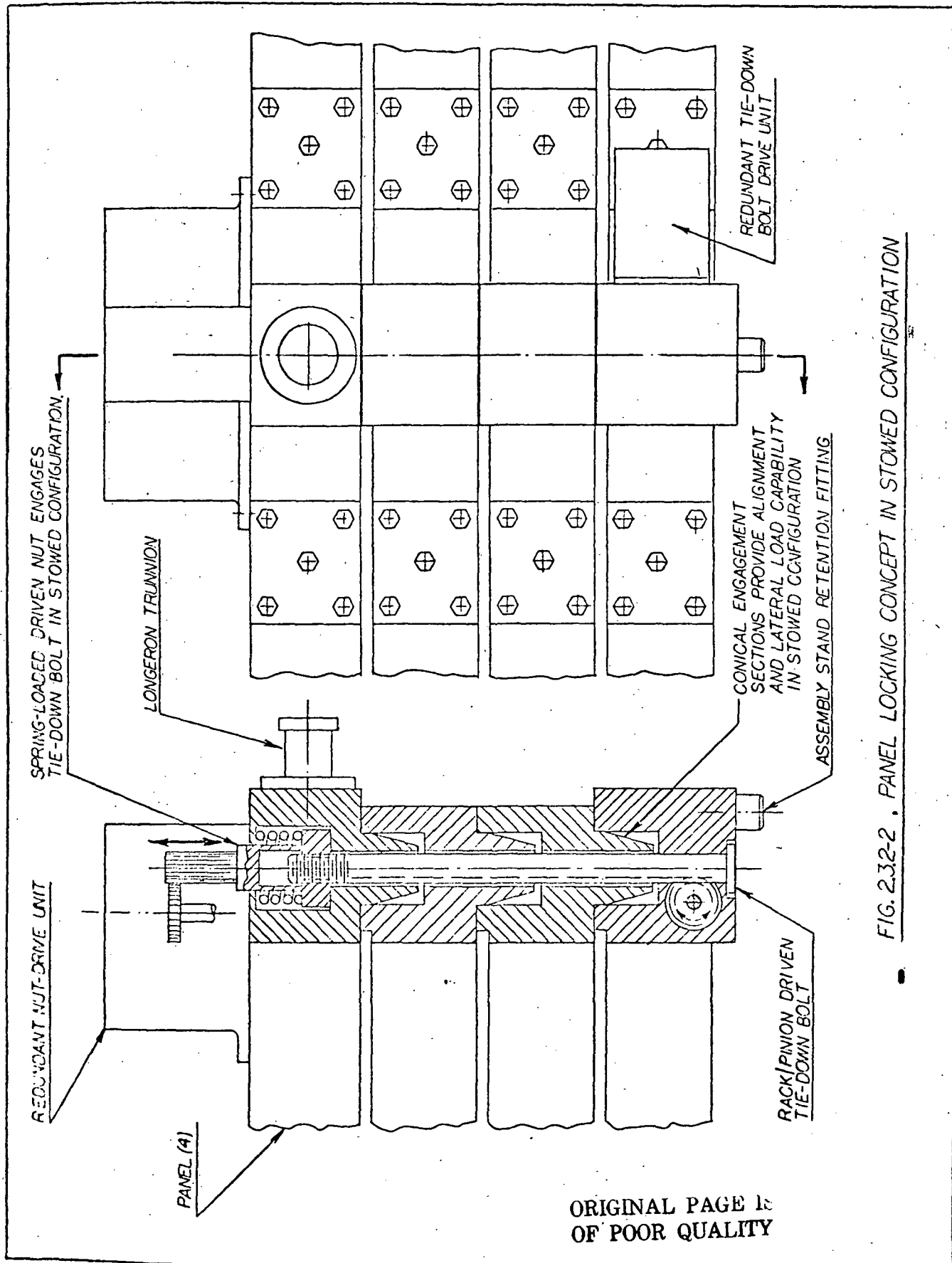


FIG. 2.32-2 . PANEL LOCKING CONCEPT IN STOWED CONFIGURATION

the remote manipulator system attached to the grapple fixture.

All payload deployment/retraction mechanisms described in detail below will be powered by dual DC permanent magnet gearhead motors coupled to a differential drive for redundancy as shown in Figure 2.3.3-1. The motors will be processed for hard vacuum operation and all gears and rotating/sliding interfaces will be "state-of-the-art" dry lubricated. In addition to providing redundancy, the differential drive inherently delivers the torque of two motors should one motor fail.

Upon command, the panel deployment sequence is initiated by activating the drive units which remove the nuts from the four tie-down bolts of the panel locking mechanisms of Figure 2.3.2-2. A limit switch, sensing nut travel, will shut off power when the tie-down bolts are free and will provide the logic signal for tie-down bolt withdrawal. As the tie-down bolts are withdrawn, the nut will follow the tie-down bolt motion, being forced against a stop by the spring element behind the nut. In this position, the nut will re-engage the tie-down bolt when the system is later retracted. A limit switch will indicate end-of-travel of the withdrawn tie-down bolt.

Figure 2.3.3-2 identifies the components located at each of the three hinged panel interfaces. The panels are connected by two hinges each located at the extreme ends. The hinges will have sufficient clearance to avoid being stressed due to static or dynamic loads during launch and ground handling operations, and will be lined with teflon bushings. The hinges are connected through two torque tubes to the main panel deploy/retract drive mechanism located midway between the hinges. In the deployed and retracted positions, the torque tubes will be preloaded against the mechanical hinge stops by providing rotational displacements of the tubes through the drive unit by some amount in excess of 180° , and below the break-away torque

ORIGINAL PAGE IS
OF POOR QUALITY

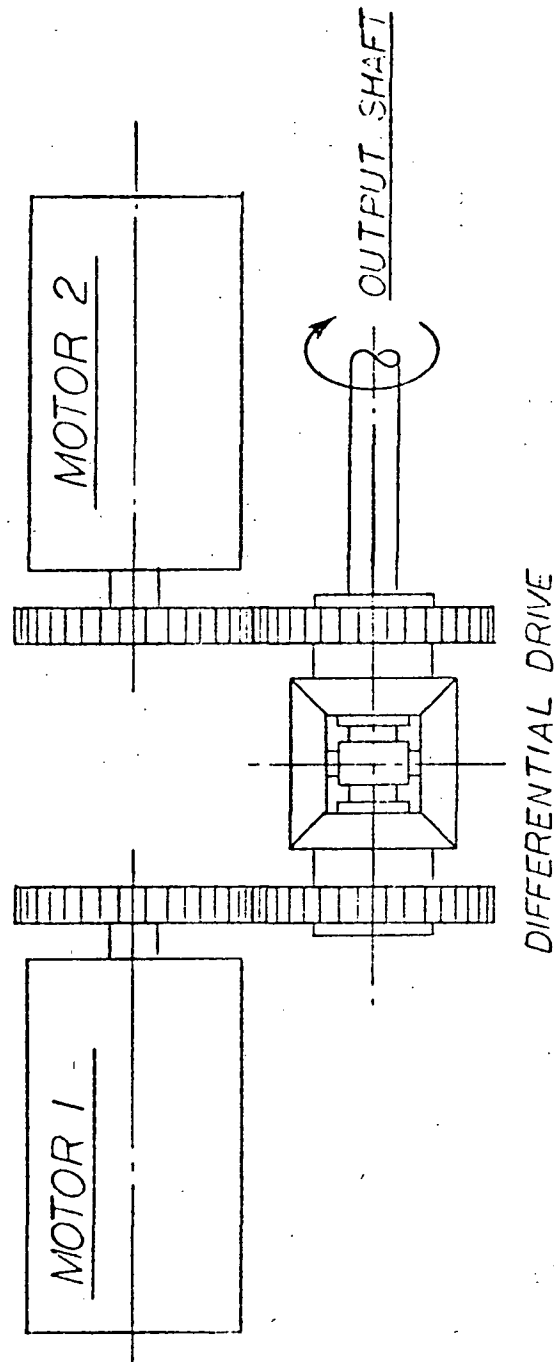


FIG. 2.3.3-1, REDUNDANT DRIVE UNIT CONCEPT

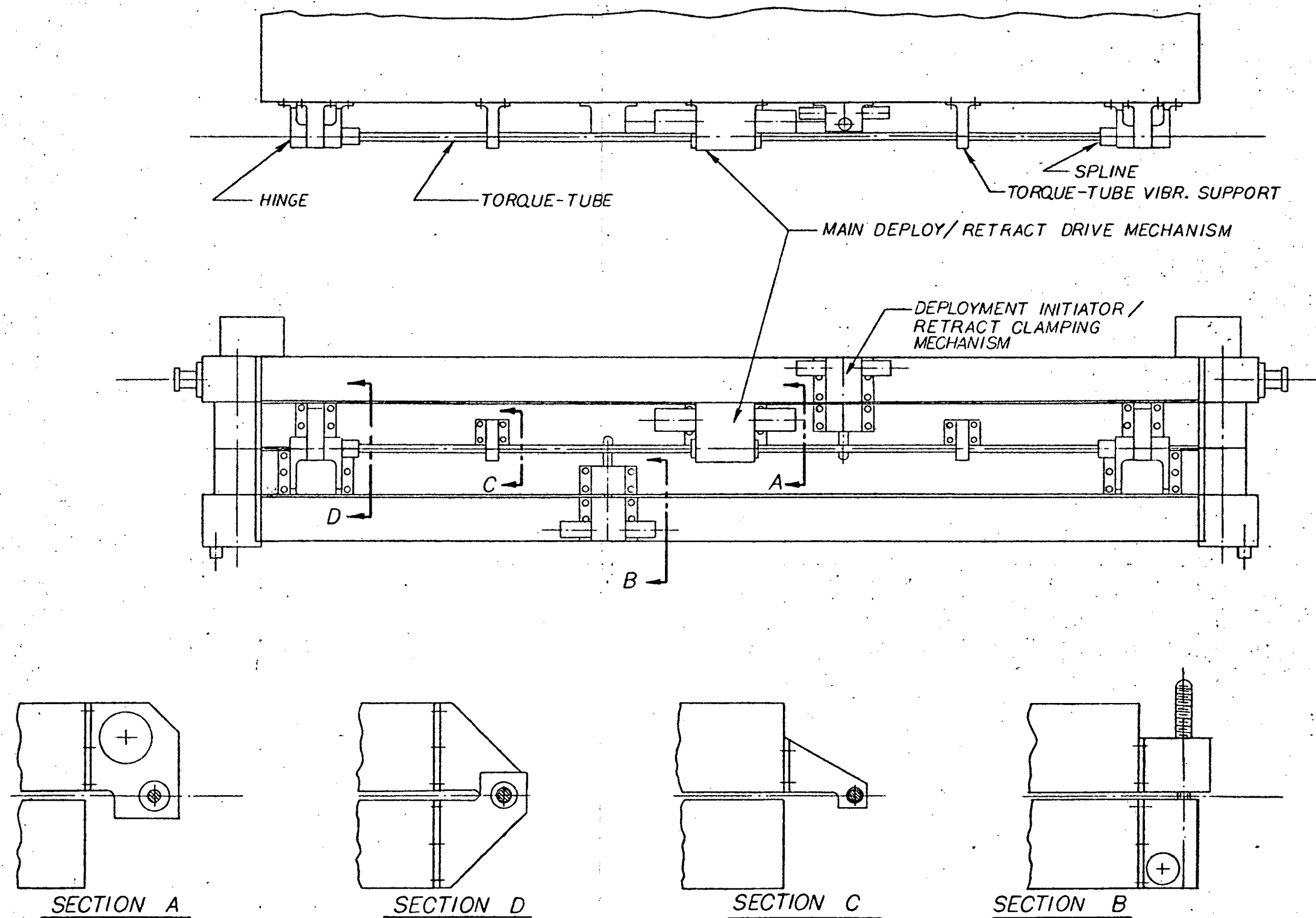


FIG. 2.3.3-2, DEPLOYMENT/RETRACTION MECHANISM ARRANGEMENT

of the drive unit and motors. The resulting energy and torque in the tubes will provide added assurance of motor operation upon command. This concept will further provide a controlled amount of constant torque holding the panels in the open position and will absorb inertia loads whenever the drive unit is activated.

Because of the great length of the individual panels, small amounts of frictional forces due to panel locking and unlocking would place unnecessarily large torque demands on the main panel deploy/retract drive unit. To prevent this, a deployment initiator/retract clamping mechanism is located between panels at the opposite end from the hinge. Shown in Figure 2.3.3-3, this mechanism will provide a large opening and closing mode force by means of a lead screw and self-aligning, passive locknut.

After the tie-down bolts have been withdrawn as described earlier, the on-board logic will command power to the deployment initiator to bring about initial opening displacements of the panels. When the lead screw has withdrawn from the locknut, a limit switch will provide a signal to the main deploy/retract drive to complete opening of the panels. Having reached the 180° open position, the mechanical hinge stop will shut off power to the motors.

The retract maneuver is essentially a reversal of the opening mode sequence with the exception that the deployment initiator/retract clamping mechanism will be running when the panels are closing in order to assure engagement of the locknuts onto the lead screws. Re-locking of the panels by the tie-down bolts and nuts will complete payload retract procedures.

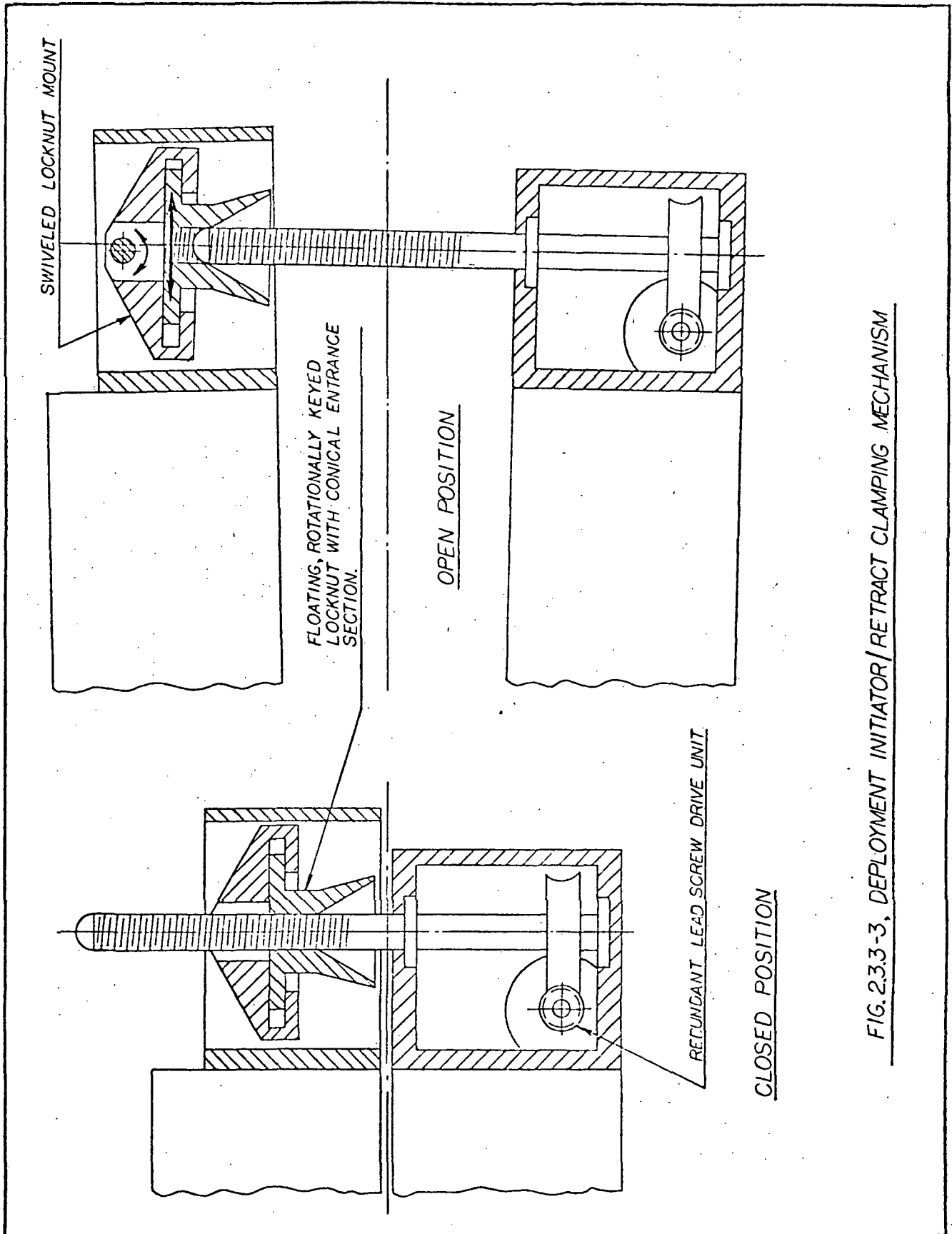


FIG. 2.3.3-3, DEPLOYMENT INITIATOR/RETRACT CLAMPING MECHANISM

2.3.4 Detector Subsystem

The passive detector subsystem will consist of approximately 110 square meters of CR-39 allyl diglycol carbonate sheets sandwiched between cold-rolled copper shielding plates as shown in Figure 2.3.4. The detector stack of uniform area density 10 gr/cm^2 will be assembled in the welded subassembly frames using protective tissue paper as shown to reduce surface damage to the outermost plastic sheets during ground handling and launch and retrieval environments. Each subassembly frame shown in Figure 2.3.1-3 will accommodate 9 separate plastic sheet stacks of approximate individual dimensions 15 x 15 inches, held in place by the bolted-on, continuous shielding plates.

In order to promote heat transfer between the copper plates through the aluminum subassembly frame, all shield-to-frame interfaces will use low-outgassing thermal grease. Detector temperature extremes will be limited by thermal control paint applied to the outer shield surfaces.

Fully assembled, each of the 72 detector subassemblies will weigh approximately 390 lbs.

2.3.5 Despin Subsystem

As a result of gravity gradient torques described in appendix A-1, the deployed payload will have an inertial angular motion rate of one revolution per orbit about an axis perpendicular to the 110 foot dimension of the assembly. Upon retracting the four deployed panels into the locked configuration, the final angular motion rate will be approximately $1.2^\circ/\text{sec}$ as described in appendix A-2.2.

In order to establish proper conditions of angular motion and position for the retracted payload such that a Shuttle recovery may be effected,

ORIGINAL PAGE IS
OF POOR QUALITY

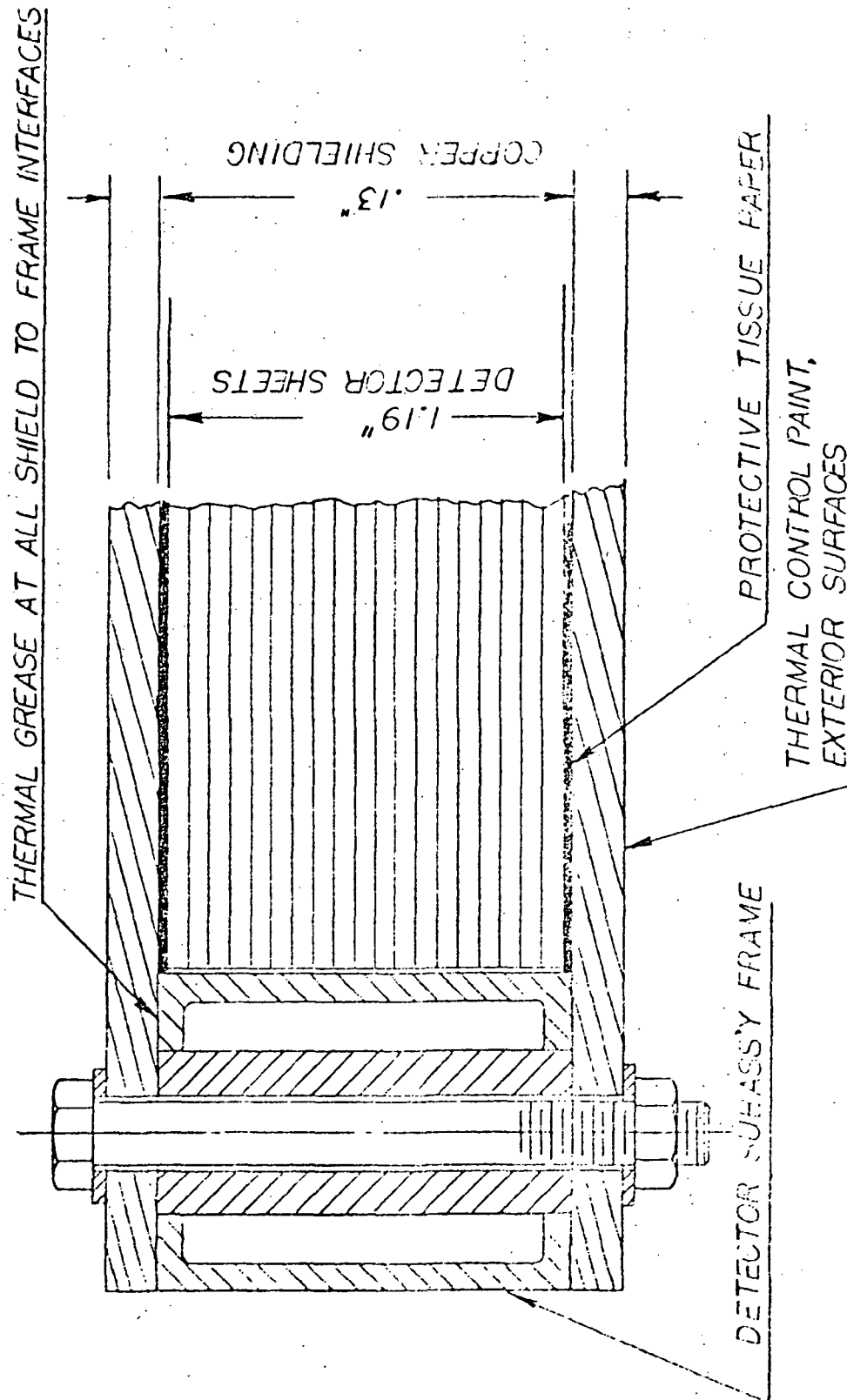


FIG.2.3.4, DETECTOR DETAIL

the payload will have a cold gas despin subsystem which can be activated by command.

The despin subsystem will be capable of holding the payload grapple fixture to a fixed angular position in space with a limit cycle which results in no greater than ± 3 inches of relative motion, and body limit cycle rates of less than $0.1^\circ/\text{second}$ about any axis after arresting initial rates. These values are taken from the Space Shuttle Payload Accommodations Handbook, Vol. IX, Rev. E.

The system will consist of a 3-axis rate gyro and conditioning electronics and will have totally redundant and separate reaction systems. Each reaction section by itself will be capable of arresting body rates. Each section will consist of one fill valve, one 300 cubic inch receiver, one regulator, and six nozzle valves. The receivers will be charged to 3600 psi nitrogen and will be initiated by a squib valve releasing gas to the regulator. The nozzle thrust will be set at one pound, but can be increased to a maximum of 12 pounds. Due to using only one set of nozzles for each axis, there will be a slight translation during rate degeneration.

For the mass properties of the retracted payload, and nozzle lever arms of 6.5 feet and 13.25 feet for the XX axis, and YY-ZZ axes, respectively, a maximum total thrust impulse of approximately 120 lb-sec is required to arrest body rates. For the 3600 psi receivers and a specific impulse for GN_2 of 60 sec ($C_F \sim 1.7$) the total gas requirement will be of the order of 2 lb. Choosing 300 cubic inch receivers will thus allow a safety margin of approximately 50%.

With these parameters of the despin subsystem, approximately 3 minutes will be required to degenerate the body rates to acceptable limits for Shuttle retrieval.

2.3.6 Telemetry/Command Subsystem

Figure 2.3.6-1 shows the electrical system block diagram. The system will be capable of receiving and executing commands to deploy and retract the payload, to activate and deactivate the despin subsystem for retrieval, and to transmit payload housekeeping information. Commands will be transmitted to the payload from the Shuttle via the S-band system. Transmission of payload housekeeping data to the Shuttle will be via a 5-watt transmitter.

The deploy/retract diagram is shown in Figure 2.3.6-2. The command to deploy the payload will apply power to the drive motors which remove the nuts from the panel lock tie-down bolts. Limit switches will then provide the signal to apply power for tie-down bolt withdrawal. When all four panel locks have been freed, the deployment initiator motors and hinge drive motors will fully extend the payload panels. The retract mode reverses the sequence of operations. After the limit switches have sensed full retraction and panel locking, the despin system will be activated to reduce payload angular motion so that recovery by the Shuttle can be effected.

2.3.7 Power Subsystem

The power subsystem will use nickel-cadmium batteries as the primary source of power and a small array of solar cells to trickle charge the batteries during the life of the mission. The power conditioning system will consist of a shunt dissipator, a battery-charge controller, and a battery-discharge regulator to maintain the system voltage at 28 vdc. The batteries will be fully charged at time of launch.

Maximum power demands are placed on the batteries initially when the payload panels are deployed, and prior to retrieval by the Shuttle when the payload will be commanded to retract. For the approximately one year period

ORIGINAL PAGE IS
OF POOR QUALITY

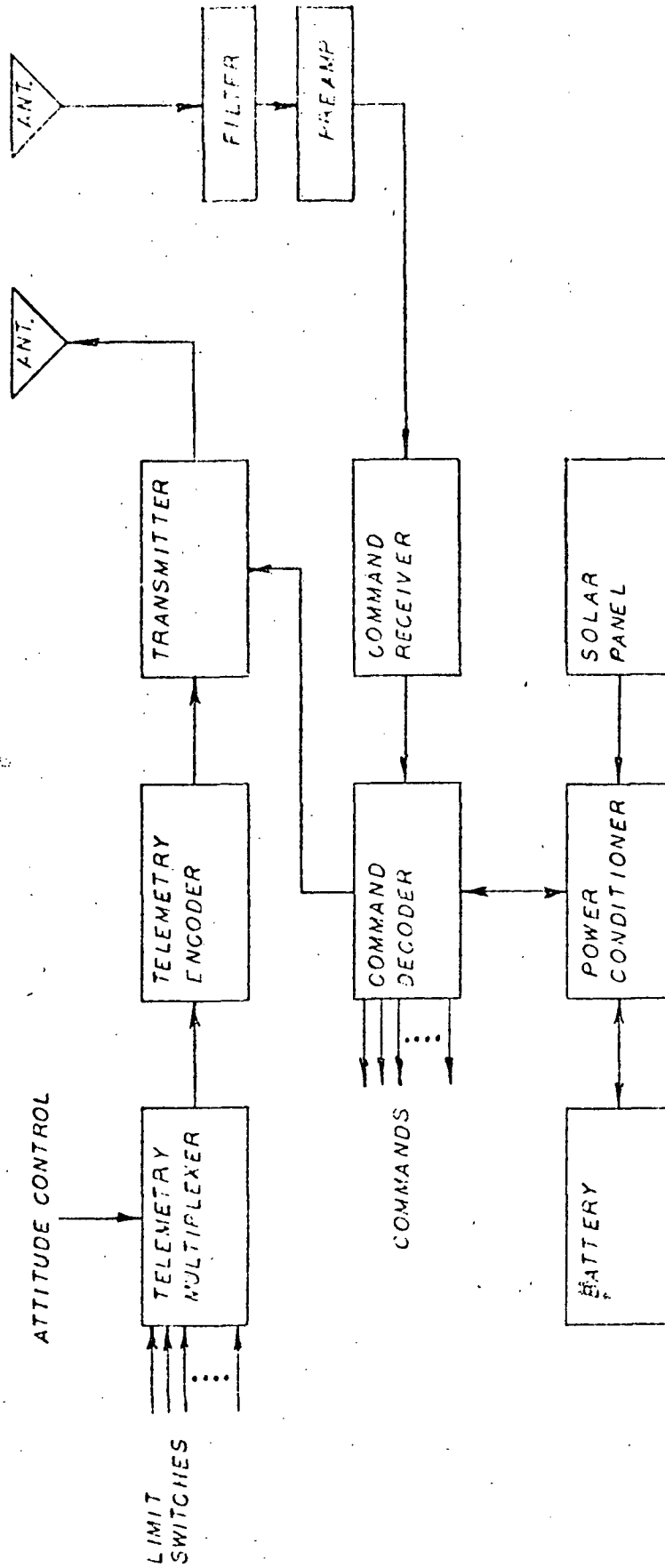


FIG. 2.3.6-1, ELECTRICAL SYSTEM BLOCK DIAGRAM



FIG. 23.6-2, DEPLOY/RETRACT LOGIC DIAGRAM

between these functions, the solar cell array will provide a small amount of power to keep the batteries charged and to operate the telemetry receiver.

For the power profile shown in Figure 2.3.7-1 the battery requirement will be approximately 120 ampere-hours which is dictated by the maximum current drawn when the tie-down bolt nut drive motors are in operation. Because of the high discharge rate capacity of nickel cadmium batteries, a current value ten times the normal discharge rate has been assumed for the two minute maximum current period.

Average power requirements for battery charging and telemetry receiver operation are approximately 5 watts. Assuming a solar cell efficiency of 10%, a view factor of $1/2\pi$, and solar energy of 1500 watts/m^2 , the solar cell-array should be approximately 0.2 m^2 .

3 Mass Properties

3.1 Weight Summary

Payload Structure and Accessories

Main Panels	3,000 lb
Yaw load structure	235 lb
Clamping and retention mechanisms	485 lb
Hinges, torque tubes and drives	90 lb
Deployment initiator and drives	45 lb
Batteries, ACS, telemetry	<u>175 lb</u>
Subtotal	4,030 lb

Detector Assembly

Detector frames	3,500 lb
Detectors	<u>24,470 lb</u>
TOTAL	32,000 lb

ORIGINAL PAGE IS
OF POOR QUALITY

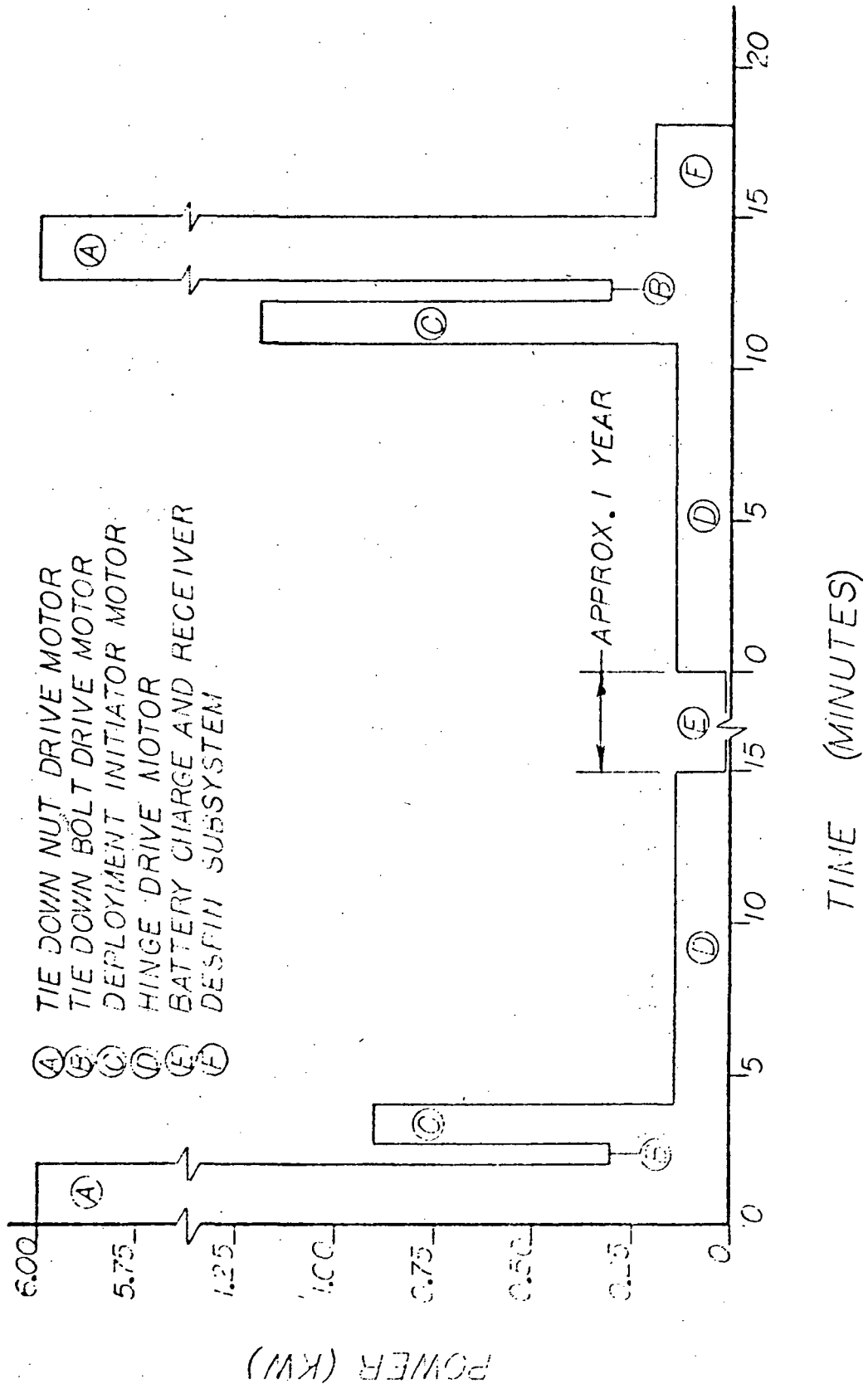


FIG. 23.7-1, POWER PROFILE

3.2 Center of Gravity Location

Geometric center in stowed and deployed configuration.

3.3 Moments of Inertia about C.G., slug-ft²,

	<u>Stowed</u>	<u>Deployed</u>
I _{X-X}	1.90 x 10 ⁴	1.86 x 10 ⁴
I _{Y-Y}	5.70 x 10 ⁴	1.00 x 10 ⁶
I _{Z-Z}	7.46 x 10 ⁴	1.02 x 10 ⁶

4 Assembly and Ground Handling

After initial buildup of the entire payload structure at the construction facility, the payload will be disassembled into discrete components for shipment to the payload installation and launch site. For ease of transportation, the four main panel frames will be disassembled for shipment also.

At the launch site, the reassembled main panel containing the yaw load structure will be positioned onto four assembly stands which support the main panel by means of the four assembly stand retention fittings identified in Figure 2.2-2. The pre-assembled detector subassemblies will then be bolted to the main panel frame. The remaining main panel frames will then be sequentially stacked and detector subassemblies fitted. An overhead, 4-ton capacity crane will be required for this operation. Integration of the deployment/retraction drive components, the despin subsystem, and the telemetry/command and power subsystem with the payload structure will complete the assembly.

Installation of the assembled payload into the Shuttle cargo bay will utilize the same concept planned for installation of the Spacelab and LDEF structures, i.e., the strong back will be used to lift the assembled payload

off the assembly stand at the payload trunnions and position it into the Shuttle cargo bay.

At the end of the mission, the above steps will be reversed and the detector subassemblies will be shipped to the experimenter.

5 Testing and Quality Assurance

5.1 Structural and Mechanical Testing

The primary payload structure will be qualified for the dynamic flight environment by analysis. Because of the structural simplicity of the four main load carrying panels, the structural response to dynamic inputs at the retention points can be accurately predicted with a high degree of confidence.

Deployment/Retraction mechanism components, Despin subsystem, and Telemetry/Command and Power subsystem components will be vibration tested using the specific location response spectra generated by analysis of the primary structure.

All active mechanical drive components will be tested for kinematics and dynamics of motion. The panel locking mechanisms will be tested on the fully assembled payload since this does not involve motion of the main panels themselves. Each complete hinge drive mechanism will be tested over the full 180° rotation by using only the hinge-adjacent U-channels of mating panels. In addition, the hinge drive mechanisms will be activated over a limited range at the time the individual panel frames are stacked on the assembly stand (without detector subassemblies). At this time the deployment initiators which are capable of lifting the empty main frame through the active initiator range will be tested for proper operation.

The despin subsystem will be scale-tested on an airbearing table to verify parameters and capability.

ORIGINAL PAGE IS
OF POOR QUALITY

5.2 Thermal-Vacuum Testing

All active mechanical drive components, the despin, telemetry/command, and power subsystem components will be subjected to thermal-vacuum tests to verify in-flight operation. The temperature response of the primary structure and detector subassemblies will be determined by exposing representative samples of the structure, coated with thermal control paint, to a sun simulation environment.

5.3 Quality Assurance

The quality assurance program will cover selection and procurement of correct parts; adequate support during the design and development stages; choice of contractors and subcontractors; and insistence on a test and inspection system to ensure that resultant hardware meets and fulfills all program requirements. Existing NASA reliability and quality-assurance publications will be used with the requirements tailored to the needs of the program.

Close coordination with responsible agencies will assure that NASA payload safety requirements are met.

6 Mission Profile and Flight Sequence Summary

Listed below are the major events and known approximate time elements outlining the mission profile.

Pre-launch operations:

- Final payload check-out at launch site (approximately 5 days)
- Installation of payload into Shuttle cargo bay and launch readiness verification

Payload orbit insertion operations:

- Payload telemetry and battery power status checkout
- Payload orbit insertion via remote manipulator system
- Tracking to establish payload orbit parameters
- Deploy payload panels via Shuttle-initiated command (approximately 15 minutes)
- Confirm panel deployment visually and via telemetry
- Record payload power status via telemetry

Payload in-orbit operations

- Occasional tracking from ground stations will be required to update orbit decay over the one year flight period
- At convenient intervals, the payload will be commanded to turn on the transmitter and provide readouts of power status and cold gas supply pressure of the despin subsystem. These commands may be initiated from the Shuttle in subsequent flights, or be ground-station-initiated.

Payload retrieval operations:

- Shuttle rendezvous tracking of payload (because of large radar cross-section of payload, tracking will be passive)
- Shuttle-initiated command to provide readout of payload power status and cold gas supply pressure.
- After visual acquisition, the Shuttle will command the payload to retract and lock the four panels. Confirmation of locking functions via telemetry. Approximately 15 minutes are required for retraction.
- Shuttle-initiated command to activate the payload de-spin subsystem. After approximately 3 minutes, the payload body rates will have degenerated to acceptable limits for Shuttle retrieval.

- After visually confirming that proper conditions of angular motion and position of the retracted payload for Shuttle retrieval have been reached, a Shuttle-initiated command will deactivate the payload despin subsystem and capture the payload via the remote manipulator system for stowage in the Shuttle cargo bay.

A P P E N D I C E S

A-1. ATTITUDE AND ORBIT DECAY

In general, the attitude of the deployed payload structure in orbit is of secondary importance to the scientific success of the mission. While detailed attitude calculations are beyond the scope of this study, considerations about the major parameters affecting attitude lead to qualitative results.

Because of the large magnitude and difference of inertia terms of the deployed structure, a relatively high value of torque is available for passively gravity-gradient stabilizing the payload with its major axis along the local vertical. The significant gravity gradient torques are given by

$$M_2 = \frac{3K}{2R^3} (I_3 - I_1) \sin 2 \theta_2 \cos \theta_1$$

$$M_3 = \frac{3K}{2R^3} (I_1 - I_2) \sin 2 \theta_2 \sin \theta_1$$

where

K = gravitation constant = 1.4075×10^{16} ft³/sec²

R = mean radius from payload to center of Earth, taken as 4,150 miles.

subscripts 1 and 2 refer to angular displacements away from the local vertical

For the inertias of the deployed payload, and a 400 km circular orbit, the maximum values for M_2 and M_3 are both approximately 2.0 ft-lb.

Aerodynamic stability and energy considerations indicate that the payload will assume an attitude which places the 110 x 15 foot dimension of the assembly normal to the velocity vector. The resulting atmospheric drag effects will thus decay the orbit. Assuming a nominal altitude for Shuttle retrieval of 296 kilometers, the NASA/GSFC Rapid Orbit Prediction

program was used to generate decay data for a one year period beginning January 1, 1982. This is an arbitrary date since it could represent any date that the payload leaves the Shuttle. The data are presented in Figure A-1.

The three conditions were that the 110 x 15 dimension be normal to the velocity vector, 2/3 of the 110 x 15 dimension be normal to the velocity vector, or the 110 x 0.7 dimension be normal to the velocity vector. The ballistic coefficients ($C_D A/M$) were $0.10426 \text{ ft}^2/\text{lbm}$, $.06951 \text{ ft}^2/\text{lbm}$, and $.0013 \text{ ft}^2/\text{lbm}$, respectively. The coefficient of drag used was 2.3 and the solar flux was 125. The table shows the starting and ending height (height after one year) for the three conditions at inclinations of 28.5 degrees and 56 degrees.

Because of a high degree of dimensional symmetry about the center of mass, the center of aerodynamic pressure will be offset from the c.g. by a relatively small amount due to the presence of the asymmetric yaw load structure. Using a conservative offset distance of 10 feet, the resulting maximum torque at the retrieval altitude of 296 km would be:

$$\begin{aligned} T &= (\text{distance}) (\text{force}) = d \left[C_D \rho \frac{V_A^2}{2} \right] \\ &= (10 \text{ feet}) \left[\frac{(2)(2 \times 10^{-14} \text{ slugs/ft}^3)(2.6 \times 10^4 \text{ feet/sec})^2}{2} (110 \times 15 \text{ feet}) \right] \\ &= (10 \text{ feet})(.02 \text{ lb}) \\ &= 0.2 \text{ ft-lb.} \end{aligned}$$

With the exception of some retention fitting and deploy/retract components, the structure and detectors use only aluminum, plastic, and beryllium copper, all non-magnetic materials. Torques resulting from the inter-

ORIGINAL PAGE IS
OF POOR QUALITY

INCLINATION = 28.5°

$C_D A/M = .0013$		$C_D A/M = .06951$		$C_D A/M = .10426$	
Start height	End height	Start height	End height	Start height	End height
312*	303	424	314.81	450	359
310	301	423	303.97	449	353.74
309	300.45	422.6	299.78	448	347.84
307	297.59	422	292.7	445	325.22
306	296.36			443	301.97
305	295.12			442	284.09

INCLINATION = 56°

$C_D A/M = .0013$		$C_D A/M = .06951$		$C_D A/M = .10426$	
Start height	End height	Start height	End height	Start height	End height
306	298.41	423	351.41	443	363.54
		413	292.95	433	291.10
		412	281.01	431	236.77

*All values in KM

Figure A-1. ORBIT DECAY

action of the payload's residual magnetism with the Earth's magnetic field should thus be small compared with the aerodynamically induced torque. Similarly, solar pressure and orbit eccentricity reduced torques will be small.

In order to assess the build-up effect of the orbit-frequency induced disturbances, the resonant frequency of payload oscillations about the gravity gradient stabilized axis must be estimated. Linearizing the gravity gradient torque about the equilibrium position, there results a restoring constant of

$$K = (M_2, M_3) / (45^\circ \times 2\pi / 360^\circ) = 2.55 \text{ ft-lb/rad.}$$

The frequency of oscillation is thus

$$f = \frac{1}{2\pi} \sqrt{K/I} = \frac{1}{2\pi} \sqrt{\frac{2.55 \text{ ft-lb/rad}}{10^6 \text{ slug-ft}^2}} = 2.54 \times 10^{-4} \text{ Hz}$$

with a period of 65.6 minutes.

The corresponding orbit period is

$$\tau = 2\pi \left(\frac{R^3}{K} \right)^{\frac{1}{2}} = 2\pi \left[\frac{(2.2 \times 10^7 \text{ feet})^3}{1.4075 \times 10^{16} \text{ ft}^3/\text{sec}^2} \right]^{\frac{1}{2}} = 91 \text{ minutes}$$

The resulting ratio of 0.721 will limit the response to approximately twice the input disturbances.

In summary, the most likely attitude of the payload will be that the 110 x 15 foot dimension is normal to the velocity vector, inclined relative to the local vertical by approximately 20 degrees maximum. The required insertion altitude for Shuttle retrieval at 296 km after one year should be approximately 440 kilometers.

A-2. DEPLOYMENT/RETRACTION DESIGN ANALYSIS

A-2.1 Panel Locking Mechanism Design

In the stowed configuration, the four large payload panels are locked together by four panel locking mechanisms located at the X,Z retention point trunnions in the manner shown in Figure 2.3.2-2. The locking force for each of these mechanisms is provided by the tie-down bolt and nut for Z-loads, and the conical engagement sections for X,Y loads. In order to provide a fixed-response structure for all static and dynamic load conditions encountered, the tie-down bolts will be preloaded to a value in excess of load conditions encountered.

From Table 7.11 of the Space Shuttle System Payload Accommodations Handbook, Vol. XIV, Rev. E, the maximum acceleration of the attach points inside the cargo bay will be 3.3 g's, and will occur during the boost phase. Since the uppermost panel is directly supported by the retention trunnions, only three panels will impose loads on the tie-down bolts. Assuming a payload dynamic load factor of 1.2, the tension load per bolt will be

$$\left(\frac{1}{4}\right)\left(\frac{3}{4}\right) (32,000 \text{ lb}) \times 3.3 \text{ g's} \times 1.2 = 23,760 \text{ lb.}$$

Thus, preloading each bolt to approximately 30,000 lb will prevent separation of the panel locking mechanism load interfaces. Applying a structural factor of safety of 4.0 to these primary tension members results in a tie-down bolt diameter of approximately 1 inch, based on a yield strength value of 150 ksi.

The equation relating tension to the required torque for power screws is given by

$$T = \frac{Fd_m}{2} \left(\frac{\rho + \pi \mu d_m}{\pi d_m - \mu \rho} \right) \frac{F \mu d_c}{2}$$

ORIGINAL PAGE IS
OF POOR QUALITY

For F = tension, = 30,000 lb

d_c = collar diameter, = 2 inches

d_m = mean screw diameter = 1 inch

ρ = pitch = 0.20

μ = coefficient of friction = 0.15,

the required torque to generate 30,000 lb tension is 680 ft-lb.

Assuming a tie-down bolt nut removal time of 2 minutes, and an overall mechanical drive efficiency of 80%, the required horsepower per drive motor is

$$HP = \frac{1}{\epsilon} \frac{T(RPM)}{5,260} = 0.81.$$

Withdrawal of the tie-down bolts from the locking mechanisms will require individual motor power of approximately .05 HP since it is only necessary to generate sufficient torque to overcome mechanism friction forces. The time required for withdrawal is 20 seconds.

A-2.2 Panel Deploy/Retract Drive Design

During deployment and retraction maneuvers the panel hinges are driven by motors connected to torque tubes and shown in Figure 2.3.3-2. The torque tubes provide elastic coupling between the panels and serve to assure a controlled torque when the panels are deployed.

As discussed in Appendix A-1, the torque requirement due to gravity gradient and atmospheric drag effects in the deployed configuration is of the order of 2.5 ft-lb. The maximum torque induced by air drag at the retrieval altitude and absorbed at the center panel hinge is given by

$$T = (\text{Total panel length})(\text{Total air drag force})$$

From Appendix A-1, the air drag force is 0.02 lb, so that $T = (110 \text{ feet})(.02 \text{ lb})/4 = .55 \text{ ft-lb}$.

Additional torque will be required due to inertial effects when the panels are retracted. In the deployed configuration, the payload will have an angular rate of 1 revolution per orbit associated with the principal axis of inertia. When the panels are retracted, application of the law of conservation of momentum will result in a stowed angular rate of

$$\omega_s = \frac{I_o \omega_o}{I_s} = \frac{1.00 \times 10^6 \text{ slug-ft}^2}{5.70 \times 10^4 \text{ slug-ft}^2} \times 1.15 \times 10^{-3} \text{ rad/sec} = .020 \text{ rad/sec}.$$

Applying this principle over the entire retraction cycle results in a torque requirement due to centrifugal forces on the center drive unit as shown in Figure A-2.2. Because of the large panel inertia coupled to the drive motors, upon initial start up the motors will essentially operate under stall current conditions. Assuming a stall current time limit of 10 seconds and a total deployment time of 10 minutes results in a deployment velocity of

$$\dot{\theta} = 180^\circ/10 \text{ minutes} = .005 \text{ rad/sec},$$

and an angular acceleration of

$$\ddot{\theta} = (.005 \text{ rad/sec})/10 \text{ seconds} = .0005 \text{ rad/sec}^2.$$

The corresponding torque required at the center of the four panels will be

$$T = I \ddot{\theta} = (10^6 \text{ slug-ft}^2)(.0005 \text{ rad/sec}^2) = 500 \text{ ft-lb}.$$

For an overall mechanical drive efficiency of 20% (high gear reduction ratio required) the motor power is thus

$$HP = \frac{1}{\epsilon} \frac{T(RPM)}{5,260} = \frac{1}{0.2} \frac{(500 \text{ ft-lb})(1/20)}{5,260} = .024 \text{ HP}.$$

ORIGINAL PAGE IS
OF POOR QUALITY

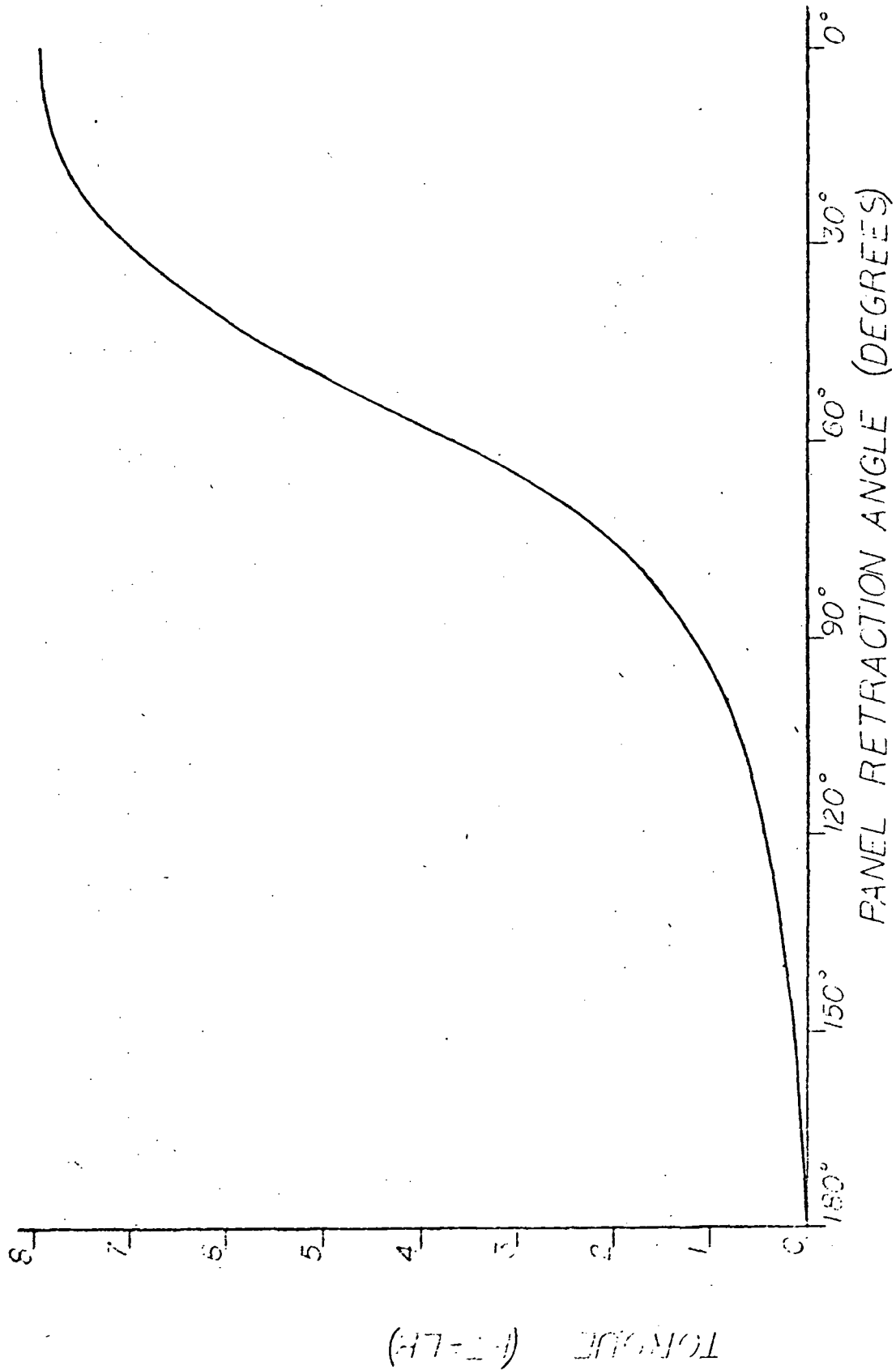


FIG. 4-2.2, TORQUE REQUIREMENT OF CENTER HINGE (RETRACTION)

The amount of kinetic energy associated with the moving panels to be dissipated at the travel stops is

$$\text{K.E.} = \frac{1}{2} I \dot{\theta}^2 = \frac{1}{2} (10^6 \text{ slug-ft}^2) (.005 \text{ rad/sec})^2 = 12.5 \text{ lb-ft}$$

A-2.3 Deployment Initiator Mechanism Design

The deployment initiator mechanisms shown in Figure 2.3.3-3 and located opposite each panel hinge are used to provide a large opening- and closing-mode force between individual panels. In addition to overcoming friction forces during opening and closing when the panels are close to the fully retracted configuration, they must also serve to provide a sufficient force to elastically overcome possible deformation in the structure setup as a result of thermal distortion.

As shown in Appendix A-3, the maximum thermal distortion of the 25-foot long continuous outer U-channel of each payload panel is expected to be of the order of 0.15 inches, the displacement being in-line with the initiator mechanism lead screw axis. Treating the total panel as a cantilever, the force required to overcome this displacement is given by $F = 3EI\delta/L^3$, where EI is the panel section modulus, and is approximately $10 \times 10^8 \text{ lb-in}^2$. The required force is thus $F = 14 \text{ lb}$.

A more demanding design parameter is the ability to lift a single 750 lb panel (without detector subassemblies) as required for ground testing of panel opening and closing mode kinematics (see Section 4). Using a $\frac{1}{2}$ -inch diameter lead screw with a pitch of 0.1 yields a torque requirement of approximately 6 foot-lb to generate a lifting force of 500 lb. The corresponding drive motor power to translate this force over 12 inches in 1 minute is approximately 0.17 HP based on a mechanical efficiency of 80%.

A-3. THERMAL DESIGN ANALYSIS

Payload temperature control will be passive and will utilize readily available thermal control paints. With the exception of the electronic systems and electric drive motors which can be insulated from the bulk payload, the structure and detector assemblies are relatively insensitive to temperature.

In the absence of internal power dissipation, payload temperature dependence can be expressed by

$$\sigma T^4 = \frac{\alpha}{\epsilon} (F_S S + F_R R) + R_E E$$

where

σ = Stefan-Boltzmann constant

T = absolute temperature of payload

α = solar absorptance

ϵ = infrared emittance

F_S = payload view factor for insulation

S = solar constant

F_R = payload view factor for planetary albedo

R = planetary albedo

F_E = payload view factor for planetary emission

E = magnitude for planetary emission

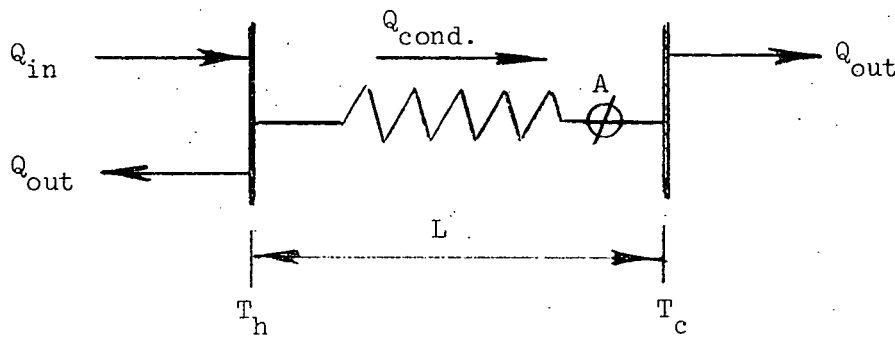
ORIGINAL PAGE IS
OF POOR QUALITY

Accurate temperature prediction will depend on the orbit inclination chosen; however, a worst case analysis may be made from the standpoint of maximum temperature excursion by assuming an approximately zero inclination orbit for the payload attitude described in Appendix A-1. Under these conditions, the view factors are approximately $F_S = 1/\pi$, $F_R = 0.1$ and $F_E = 0.4$

Selecting a W.P. Fuller Al - Silicon paint, No. 172-A-1, with $\alpha = 0.28$ and $\epsilon = 0.25$, and letting $S = 444 \text{ Btu/hr-ft}^2$, $R = 0.3S$, and $E = 77 \text{ Btu/hr-ft}^2$,

there results an average payload temperature of +35°F.

The payload temperature will drop once per orbit during the shadow period. An estimate of the temperature variation may be obtained by calculating the net heat loss per orbit. As shown in Figure 2.3.4, the two copper shielding plates of the detector subassemblies are conductively coupled to each other by means of rectangular aluminum channels making up the detector subassembly frame, and thermal grease at all aluminum to copper interfaces. The heat transfer parameters across the detector assembly may then be modeled as follows



where

$$\begin{aligned} Q_{in} &= \alpha(F_S S + F_R R) \\ Q_{out} &= \epsilon \sigma T^4 \\ Q_{cond} &= \frac{kA}{L} (T_h - T_c). \end{aligned}$$

Writing the heat balance equation and solving for the temperature difference across the assembly results in

$$\Delta T = \frac{\alpha(F_S S + F_R R)L}{2Ak}$$

Per unit area of copper plate, the aluminum frame parameters are:

$A = .023 \text{ ft}^2$, $L = 0.10 \text{ feet}$, $k = 120 \text{ Btu/hr-ft-}^\circ\text{F}$, with a resulting

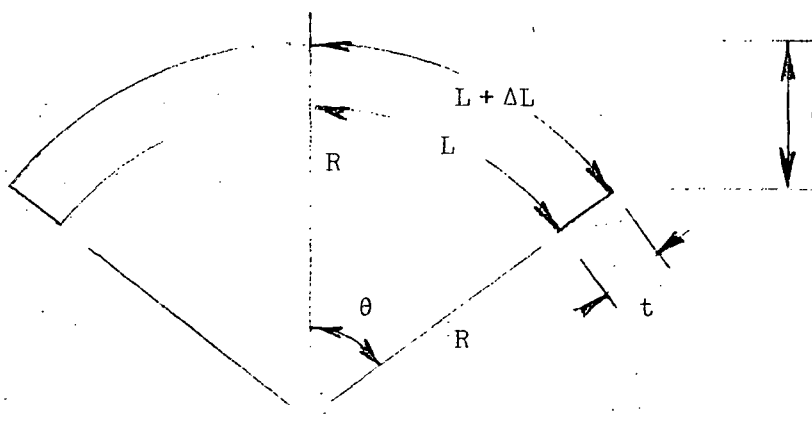
temperature difference of 0.8°F. Because of this small temperature difference, the CR-39 detector plates do not contribute to the net heat transfer as their mode of heat transfer is essentially that of radiation only.

During the approximately 45 minute shadow period, the net heat loss per unit area detector assembly is given by

$$\Delta Q = (2\sigma\epsilon T^4 - \epsilon F_E E)\Delta t$$

Using an average temperature of +20°F, the corresponding heat loss is 28 Btu. Finally, equating this heat loss to the thermal capacitance of the two copper plates results in a temperature drop of 23°F.

To assure functioning of the retract subsystem of the payload, deformation of the structure due to thermal distortion must be investigated. The most predominant distortion will result from solar insolation and planetary albedo onto one side of the continuous 25-foot long outer U-channel of each payload panel. The problem may be idealized as shown in the following sketch



From geometric relations, $L/R = (L + \Delta L)/(R + t) = \theta$, and $R = Lt/\Delta L$. Also, $\delta = (1 - \cos\theta)R$. For a thermal expansion coefficient, e , and temperature difference across the span of ΔT , the incremental length is $\Delta L = Le\Delta T$. Combining these relationships yields

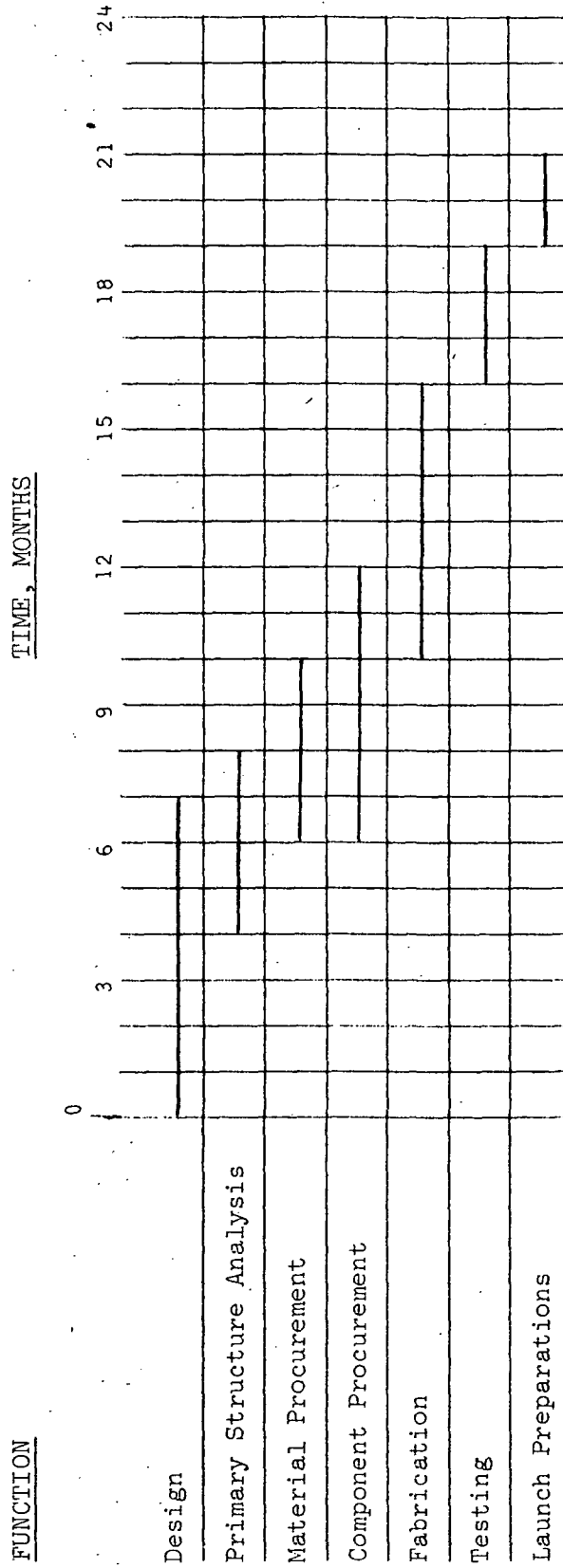
$$\delta = \left[1 - \cos\left(\frac{Le\Delta T}{t}\right) \right] \frac{t}{e\Delta T}$$

The temperature difference may be determined by the same method used for the detector assembly. For the properties of the U-channel, this value is found to be 1.8°F which, when used with $e = 13 \times 10^{-6}$ in/in °F for aluminum, yields $\delta = 0.14$ inch. The method of accommodating this deflection is described in Appendix A-2.

ORIGINAL PAGE IS
OF POOR QUALITY

A-4. SCHEDULE

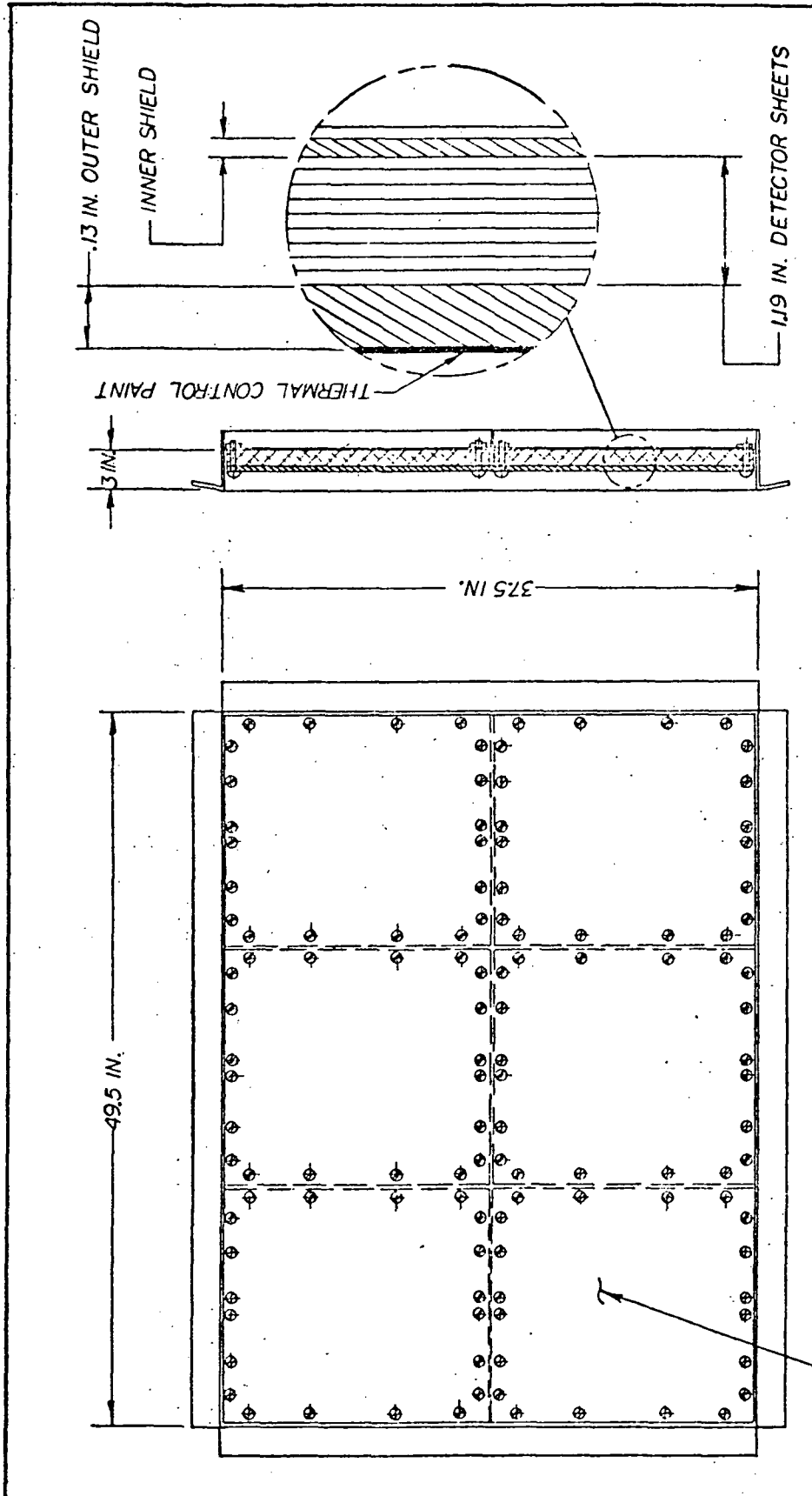
The chart below presents an overview of major functions and corresponding time elements in the development of the EPIC payload.



A-5. LDEF OPTION

The passive detector subsystem described in Section 3.4 is readily adaptable for mounting in a standard 3-inch peripheral tray assembly for use in the Long Duration Exposure Facility (LDEF). Figure A-6 shows details of the mounting arrangement. Each such tray assembly would provide approximately 1.10 square meter detector area.

Depending on the amount of shielding available from other experiments in the LDEF module facing the detector assembly, the total weight of each LDEF detector assembly would be between 165 and 230 lb.



6 SEPARATE DETECTOR SHEET STACKS OF INDIV. SIZE 16.40 X 18.65 IN.,
COVERED BY FULL INNER AND OUTER SHIELDS 49.4 X 37.4 IN., ALL
SECURED TO LDEF TRAY FLOATING PLATE NUTS WITH 10-32 SS NON-MAGN BOLTS.

FIG. A-6 EPIC PASSIVE DETECTOR

MOUNTED IN STANDARD 3-INCH LDEF PERIPHERAL TRAY ASSEMBLY